CENTRAL RESEARCH LIBRARY
DOCUMENT COLLECTION

[redacted]

ORNL-1503
Progress

AEC RESEARCH AND DEVELOPMENT REPORT

MARTIN MARIETTA ENERGY SYSTEMS LIBRARIES
3 4456 0353309 5

DECLASSIFIED
CLASSIFICATION CHANGED TO:
BY AUTHORITY OF: AEC - 6-12-62
BY: A. Bowman 8-10-62

LABORATORY RECORDS
1954

METALLURGY DIVISION

QUARTERLY PROGRESS REPORT

FOR PERIOD ENDING JANUARY 31, 1953

CENTRAL RESEARCH LIBRARY
DOCUMENT COLLECTION
LIBRARY LOAN COPY
DO NOT TRANSFER TO ANOTHER PERSON
If you wish someone else to see this document, send in name with document and the library will arrange a loan.

OAK RIDGE NATIONAL LABORATORY
OPERATED BY
CARBIDE AND CARBON CHEMICALS COMPANY
A DIVISION OF UNION CARBIDE AND CARBON CORPORATION
UCC
POST OFFICE BOX P
OAK RIDGE, TENNESSEE

[redacted]

This document contains Restricted Data as defined in the Atomic Energy Act of 1946. Its transmittal or the disclosure of its contents in any manner to an unauthorized person is prohibited.

[redacted]

[redacted]

ORNL-1503

This document consists of 52 pages.

Copy 5 of 140 copies Series A

Contract No W-7405-eng-26

METALLURGY DIVISION

QUARTERLY PROGRESS REPORT

for Period Ending January 31, 1953

J. H. Frye, Jr., Director

EDITED BY

W. H. Bridges

DATE ISSUED

MAR 18 1953

OAK RIDGE NATIONAL LABORATORY
Operated by
CARBIDE AND CARBON CHEMICALS COMPANY
A Division of Union Carbide and Carbon Corporation
Post Office Box P
Oak Ridge, Tennessee

[redacted]

MARTIN MARIETTA ENERGY SYSTEMS LIBRARIES

3 4456 0353309 5

[redacted]

[redacted]

ORNL-1503
Progress

INTERNAL DISTRIBUTION

1. C. E. Center
2. Biology Library
3. Health Physics Library
4. Metallurgy Library
5-6. Central Research Library
7. Reactor Experimental Engineering Library
8-13. Central Files
14. C. E. Larson
15. W. B. Humes (K-25)
16. L. B. Emlet (Y-12)
17. A. M. Weinberg
18. E. H. Taylor
19. E. J. Murphy
20. E. D. Shipley
21. J. H. Frye, Jr.
22. F. C. VonderLage
23. R. C. Briant
24. J. A. Swartout
25. S. C. Lind
26. F. L. Steahly
27. A. H. Snell
28. A. Hollaender
29. M. T. Kelley
30. K. Z. Morgan
31. J. S. Felton
32. A. S. Householder
33. C. S. Harrill
34. C. E. Winters
35. D. S. Billington
36. D. W. Cardwell
37. E. M. King
38. A. J. Miller
39. D. D. Cowen
40. P. M. Reyling
41. W. H. Bridges
42. G. C. Williams
43. L. K. Jetter
44. E. J. Boyle
45. W. D. Manly
46. C. D. Susano
47. W. W. Parkinson
48. R. J. Gray
49. B. S. Borie
50. D. C. Vreeland
51. E. E. Stansbury
52. G. P. Smith
53. J. E. Cunningham
54. R. S. Crouse
55. R. E. Adams
56. J. H. Erwin
57. J. O. Betterton, Jr.
58. L. D. Dyer
59. G. M. Adamson
60. E. S. Bomar
61. F. H. Eckert
62. T. W. Fulton
63. W. J. Fretague
64. R. B. Oliver
65. J. T. Howe
66. T. H. Blewitt
67. W. E. Taylor
68. J. H. Crawford, Jr.
69. J. C. Wilson
70. H. W. Savage
71. E. E. Hoffman
72. W. J. Leonard
73. J. A. Milko
74. J. M. Warde
75. E. C. Cruetz (consultant)
76. E. P. Wigner (consultant)
77. W. W. Grigorieff (consultant)

[redacted]

[redacted]

[redacted]

EXTERNAL DISTRIBUTION

78-85. Argonne National Laboratory
86-93. Atomic Energy Commission, Washington
94. Battelle Memorial Institute
95-98. Brookhaven National Laboratory
99. Brush Beryllium Company (N. W. Bass)
100-103. Carbide and Carbon Chemicals Company (Y-12)
104-105. Knolls Atomic Power Laboratory
106-107. General Electric Company, Richland
108-110. General Electric Company (ANPP)
111. Hanford Operations Office
112. Idaho Operations Office (Phillips Petroleum Co.)
113-116. Los Alamos
117. Massachusetts Institute of Technology (Kaufmann)
118-119. New York Operations Office
120. Patent Branch, Washington
121. Savannah River Operations Office, Wilmington
122-136. Technical Information Service, Oak Ridge
137-140. University of California Radiation Laboratory

[redacted]

[redacted]

[redacted]

Reports previously issued in this series are as follows

ORNL-28	Period Ending March 1, 1948
ORNL-69	Period Ending May 31, 1948
ORNL-407	Period Ending July 31, 1949
ORNL-511	Period Ending October 31, 1949
ORNL-583	Period Ending January 31, 1950
ORNL-754	Period Ending April 30, 1950
ORNL-827	Period Ending July 31, 1950
ORNL-910	Period Ending October 31, 1950
ORNL-987	Period Ending January 31, 1951
ORNL-1033	Period Ending April 30, 1951
ORNL-1108	Period Ending July 31, 1951
ORNL-1161	Period Ending October 31, 1951
ORNL-1267	Period Ending January 31, 1952
ORNL-1302	Period Ending April 30, 1952
ORNL-1366	Period Ending July 31, 1952
ORNL-1437	Period Ending October 31, 1952

[redacted]

[redacted]

[redacted]

CONTENTS

	Page
SUMMARY	1
PHYSICAL METALLURGY OF REACTOR MATERIALS	2
Thorium Alloy Development	2
Thorium-vanadium alloys	2
Thorium-silicon alloys	3
Physical Properties of Thorium	3
Radiation Damage of Thorium	4
LITR irradiation experiments	4
MTR irradiation experiments	4
Properties of Pure Metals	4
HRP METALLURGY	5
Service to Corrosion and Engineering Groups	5
Welding of Type 347 Stainless Steel	5
Radiation Damage Studies	5
Properties of Titanium	5
Fabrication	5
HRE recombiner	5
Riveting of second HRE impeller	6
ANP METALLURGY	6
Static Corrosion	6
Fluoride corrosion	6
Liquid metal corrosion	9
Dynamic Corrosion	13
Zirconium fluoride base fuels	13
Hydrofluorinated fulinak No. 14	18
Additives to fluorides	18
Inserted corrosion samples	18
Crevice corrosion	19
Temperature variations	19
Miscellaneous loops	19
Welding	19
Cone-arc welding	19
Resistance welding	20
Fabrication of heat exchanger test units	22
High-temperature brazing alloy evaluation program	23
Brazing of copper to Inconel	26

[redacted]

[redacted]

[redacted]

Fabrication 27
Control rods 27
ARE shielding plugs 27
Tower shielding facility safety rods 27
Solid-phase bonding 28
Special alloy fabrication 28
Columbium research 28
ANP radiators 30
Mechanical Testing 30
Uranium 30
Thorium 30
Inconel 31
Type 316 stainless steel 31
Physical Chemistry 31
Studies of surface rearrangements on a single crystal of copper in contact with a saturated solution of copper in bismuth 31
Future work 34

CERAMICS RESEARCH 35

Ceramic Coatings for Metals 35
Radiator coatings (ANP) 35
Fluoride-resistant coatings 35
High-boron coatings 35
Radiation Damage Studies 35
Development of Cermets for Reactor Components 35
Oxide Ceramics 36
Thorium oxide 36
Uranium oxide 36
Fabrication of Spheres from Ceramic Materials 36
Vapor Coating of Beryllium Oxide 36
Insulating End-Cap Development 37
Uniformity of Beryllium Oxide Blocks 37
Petrographic Examination of Fluorides 38

REACTOR COMPONENT FABRICATION 40

Thorium-Uranium Fuel Element 40
Fabrication of Uranium-Aluminum Alloy Components 41
MTR experimental studies 41
Studies to eliminate flux entrapment 41
MTR replacement fuel and control rod elements 43
Convair fuel and control rod elements 45
NAA Alclad uranium-aluminum alloy plates 46

[redacted]

[redacted]

METALLURGY DIVISION QUARTERLY PROGRESS REPORT

SUMMARY

PHYSICAL METALLURGY OF REACTOR MATERIALS

Investigation of the effect of vanadium additions (up to 8.5%) and silicon additions (up to 0.1%) on the properties of thorium has shown that neither of these is a potent strengthener. The effect of heat treatment on the properties of the vanadium alloys will be investigated.

Expansivity measurements on thorium have not shown any discontinuity in the temperature range 1325 to 1450°C, where a sharp increase in electrical resistivity had been noted previously. Further refined tests are planned.

Radiation damage tests on thorium specimens are now under way in the LITR. Specimens of unalloyed thorium and of 99% Th–1% U^{235} alloy are being prepared for MTR exposure.

ANP PROGRAM

The phenomenon of crevice corrosion in fluoride salts has been investigated in static corrosion tests. A series of screening tests has been conducted to find a material for use as valve seats, pump bearings, and shaft coatings when in contact with fluoride fuels. The compatibility of BeO and NaK is also being examined. Alloys of sodium and lead have been used in corrosion tests, and it was found that these alloys have less corrosive attack on the structural metals than lead has.

Dynamic corrosion testing of the fluoride fuels in Inconel and other structural metals has continued. The main effort has been on determining the various factors affecting fluoride corrosion, such as the batch size of the fluoride fuel, the cleaning procedure for the loop, and various additions to the fuel. It has been confirmed that additions of ZrH_2 and TiH_2 minimize the attack of the fluoride fuels on Inconel.

Cone-arc welding is now being applied to the construction of heat exchanger subassemblies for possible application in the ANP Program. It was found that dished headers impose a new problem of unequal arc distances in cone-arc welding. Some preliminary results have shown that stainless-steel-clad fuel elements can be spot welded. Cold-rolled thorium has been spot welded and sufficient tests have been conducted to show that the shear stress of the welded joint increases with welding current and then levels off. This is quite similar to the spot welding of plain carbon steels. The Nicrobrazing of large complicated radiators is continuing. In the high-temperature-brazing evaluation program, the corrosion behavior of several brazing alloys in various media has been studied. The high-temperature mechanical properties of some of the brazed joints are presented in the text.

Control rod inserts, which are a mixture of boron carbide and iron, are being prepared by powder metallurgy for the GE-ANP Materials Section. The control rod inserts must be metallurgically bonded to the outside stainless steel tube, and various brazing alloys are being studied for this application. Special heats of high-purity Inconel are being prepared for corrosion tests. The oxidation characteristics of columbium are being studied. In an ANP type of radiator, the efficiency would be much greater if it were possible to use fins having a high thermal conductivity. Therefore a program of research has been initiated to study means of cladding copper to give it oxidation resistance, and brazing alloys are being developed to attach the clad fins to the high-temperature-alloy tubing.

Creep tests on uranium and thorium are continuing, and the effect of extrusion rate on the creep properties of thorium is being studied. The study of the effect of environment on the creep and stress-rupture properties of Inconel and stainless steels is continuing.

A study has been made of the influence of the variation of surface free energy with orientation in determining the surface topography of a metal single crystal. It was found that considerable surface rearrangement occurred on a copper crystal immersed in a saturated solution of copper in bismuth at 400°C. This rearrangement resulted in the formation of small polyhedral prominences, called pimars, on the crystal surface. The major bounding faces of the pimars consisted of (111) and (110) crystallographic planes. A tentative hypothesis was proposed to explain the experimental results. The basic assumptions of the

hypothesis are (1) in a copper crystal there exist variations in surface free energy with orientation that provide the driving force for the observed surface rearrangement, (2) pimar formation is a nucleation and growth phenomenon, a nucleation energy being required to initiate growth.

CERAMICS

Test work indicates that a ceramic coating containing 10% boron, developed in the Ceramic Laboratory, can be successfully applied to a thickness of 15 mils on mild steel that is up to $\frac{1}{16}$ in. in thickness. A peculiar banding structure was observed in quartz specimens irradiated with a cobalt source. In the ceramic fuel element studies, annular rings have been formed from a cermet composition containing 70% Cr–30% Al_2O_3, about 8% UO_2 is included in sandwich form in the compact. Further accomplishments on ceramic fuels include the development of a SiC-Si body by using special techniques, preparation of USi_2 bodies, and the development of a design for an in-reactor high-temperature test rig. Work was carried out on the preparation of ThO_2 and UO_2 bodies intended for reactor service. An investigation of the vapor decomposition method for the application of coatings to ceramics was started. An investigation was begun on the development of insulating end caps for Hanford-type slugs. A study of the physical structure of the BeO blocks intended for the ARE was made as an aid to the interpretation of the BeO-NaK compatibility tests. Petrographic studies included the examination of fluoride mixtures and other combinations in connection with ANP fuel investigations. Petrographic investigation of the monohydrate of UO_3 is in progress.

REACTOR COMPONENT FABRICATION

Cladding experiments are in progress to establish the technical feasibility of a "package" reactor design that features the use of thorium-uranium alloy fuel elements. Preliminary work indicates that the thorium-rich alloy is easily prepared and can be readily hot or cold worked by conventional methods, also, that the alloy can be metallurgically bonded to both aluminum and zirconium for construction of flat-plate-type elements. Attempts are being made to clad the alloy with stainless steel.

Alclad plates with 98.8 wt % thorium and highly enriched uranium cores have been fabricated and forwarded to the MTR for irradiation testing.

Initial design and fabrication studies to improve the operational performance of the MTR are complete. Results indicate that a gain in excess reactivity of 3 to 4% is possible by judicious modifications in design and techniques of manufacturing the fuel elements.

It is proposed to replace the lower stainless steel section in the shim control rod with an aluminum extrusion to reduce fabrication cost. The change will not adversely affect either operational control or the mechanical stability of the rod.

PHYSICAL METALLURGY OF REACTOR MATERIALS

E. J. Boyle

THORIUM ALLOY DEVELOPMENT

J. A. Milko

The alloy development program for improving the corrosion resistance and mechanical properties of thorium has continued. Analyses for the thorium-vanadium alloys, the mechanical properties of which were reported previously,[1] are now available and are listed in Table 1.

Concurrently with the preparation of thorium-vanadium alloys, alloys of silicon with Ames thorium were prepared by arc melting. Results of the effect of small additions of silicon on the mechanical properties of Ames thorium are listed in Table 2.

Thorium-Vanadium Alloys. The effects of vanadium on thorium are shown in the data of Table 1. Additions of about 0.6% to 1.2% of vanadium to thorium seem to lower the hardness and strength properties. This appears to be either a deoxidation action on the thorium by the vanadium or a

[1] J. A. Milko, *Met. Div. Quar. Prog. Rep. Oct 31, 1952*, ORNL-1437, p. 4.

removal of carbon from a probable solid solution by the formation of vanadium carbide.

Additions of vanadium above about 1.2% appear to harden the thorium. However, the rate of hardening, or, for that matter, of strengthening, is not too marked. Therefore, by disregarding any probable effects of heat treatment, it may be concluded that vanadium does not appear to be a potent alloying element for thorium.

Thorium-Silicon Alloys. Additions of small amounts of silicon to Ames thorium tend to increase the strength properties and hardness gradually. Ductility, as measured by per cent elongation and reduction of area, is lowered gradually by the addition of small amounts of silicon. The data are presented in Table 2.

It seems desirable at this time for additional alloys of higher silicon content to be prepared for study. Knowledge of properties of such alloys would be directly applicable to several problems relating to reactor material design.

PHYSICAL PROPERTIES OF THORIUM

R. E. Adams

Previous work indicated that a sharp increase in the electrical resistance of thorium occurs in the

TABLE 1. EFFECT OF VANADIUM ON THE PROPERTIES OF AMES THORIUM

Annealed for ½ hr at 750°C after cold swaging about 50%

CHEMICAL COMPOSITION (%)			TENSILE STRENGTH (psi)	YIELD STRENGTH AT 0.2% OFFSET (psi)	PROPORTIONAL LIMIT (psi)	ELONGATION IN 1.5 in. (%)	REDUCTION OF AREA (%)	ROCKWELL H HARDNESS
V	C	Th[a]						
0.39	0.038	Balance	30,900[b]	20,000[b]	16,200[b]	47.0[b]	57 0[b]	78
0.59	0.036	Balance	29,300[c]	17,900[c]	13,700[c]	57.0[c]	64 0[c]	65
1.17	0.033	Balance	27,400[c]	16,600[c]	13,700[c]	51.0[c]	62.0[d]	75
3 33[e]	0.040[e]	Balance	33,600[d]	16,300[d]	11,400[d]	34.0[d]	55 0[d]	81
6.30[e]	0.087[e]	Balance	39,500[b]	20,400[b]	12,100[b]	26.0[b]	40.0[b]	93
8.54	0.042	Balance	36,700[b]	20,200[b]	12,700[b]	28.0[b]	50.0[b]	100

[a]Also contains trace impurities of Be, Al, Fe, N, Ca, Mg, B, Cd, and Zn.
[b]Average of four tests.
[c]Average of three tests.
[d]Average of two tests.
[e]Values appear to be high and will be checked.

TABLE 2. EFFECT OF SILICON ON THE PROPERTIES OF AMES THORIUM

Annealed for ½ hr at 750°C after cold reduction of about 85%

CHEMICAL COMPOSITION (%)			TENSILE STRENGTH (psi)	YIELD STRENGTH AT 0 2% OFFSET (psi)	PROPORTIONAL LIMIT (psi)	ELONGATION IN 2 in (%)	REDUCTION OF AREA (%)	HARDNESS	
Si	C	Th[a]						Rockwell H	VHN
0 032	0 032	Balance	25,700[b]	15,000[b]	9,600[b]	51 0[b]	54 0[b]	89[c]	65[c]
0 077	0 037	Balance	27,700[b]	16,700[b]	11,000[b]	44 0[b]	54 0[b]	94[c]	72[c]
0 110	0 041	Balance	29,800[b]	18,700[b]	12,700[b]	42 0[b]	48 0[b]	95[c]	72[c]

[a]Also contains trace impurities of Be, Al, Fe, N, Ca, Mg, B, Cd, and Zn.
[b]Average of two tests
[c]Average of ten readings.

temperature range of about 1325 to 1450°C. In an effort to ascribe a reason for this, investigations are being made to learn whether any other properties of thorium undergo changes in this temperature region.

Preliminary experiments have been made to measure the coefficient of thermal expansion of thorium at high temperatures. The data obtained thus far indicate that no significant discontinuities occur in the thermal expansion vs. temperature curve between about 900 and 1600°C. Since the test methods were somewhat crude, the coefficients of expansion of thorium are not accurately known. Some improvements in technique have been adopted, and later tests with iron have indicated that the phase transformation between alpha and gamma iron, and between gamma and delta iron, are clearly indicated. Additional tests with thorium will be made in the near future.

RADIATION DAMAGE OF THORIUM

R. E. Adams R. H. Kernohan[2]

A study of the effects of neutron irradiation on the properties of thorium is being carried out. Although no information has been obtained from these experiments, as yet, the status and scope of the program will be described here.

LITR Irradiation Experiments. Several thorium test specimens are now being irradiated in the LITR at an approximate flux of 4×10^{12} neutrons/cm^2 sec. A detailed description of the specimens was given in ORNL-1366.[3] Irradiation of the cylindrical and the hardness test specimens started on August 19, 1952, and the tensile and impact specimens were put in the reactor on December 1, 1952. The specimens will be exposed for six months.

MTR Irradiation Experiments. Plans have also been made for irradiation of thorium in the MTR. Specimens will be irradiated at a flux of about 10^{14} neutrons/cm^2·sec. One set of specimens will be exposed for six months, a duplicate set will be exposed for one year. The specimens will be canned in capsules containing liquid NaK to provide good heat transfer between the specimens and the capsule walls.

Each set of specimens will contain the following samples

1. two cylindrical test specimens, 0.204 in. in diameter and 4 in. long, which will be used to study changes in dimensions, dynamic elastic modulus, electrical conductivity, and thermal conductivity,
2. four impact test specimens, 0.204 in. in diameter and $4\frac{3}{4}$ in. long, each of which can be broken in four places,
3. twelve hardness test specimens, 0.204 in. in diameter and $\frac{1}{8}$ in. thick, which are for study of changes in hardness and possible effects of postirradiation annealing.

A test program is also being planned for investigating the effects of irradiation damage in thorium containing U^{235} as an alloying addition.

Tentatively, it is planned to irradiate a 99% Th–1% U^{235} alloy, and to approximately duplicate the present experiments scheduled for MTR irradiation.

PROPERTIES OF PURE METALS

W. J. Fretague

The Mechanical Testing group has performed elevated-temperature tensile tests on specimens made from six induction-melted nickel rods, which were described in a previous report.[4] Variations in the impurity content of the individual melts affected the physical properties of the material to such a degree as to make the data noninterpretable for the purpose for which the experiments were designed. A purchase order has been placed with the Vacuum Metals Corp. for 20 ft of $\frac{7}{8}$-in.-dia "Nivac" (high-purity, gas-free nickel). This material is produced in 200-lb ingots, and therefore it is possible to obtain specimens that are more homogeneous than those obtained from individual melts. When this material is delivered the experiments will be repeated.

[2] Solid State Division.

[3] R. E. Adams, *Met. Div Quar. Prog. Rep. July 31, 1952*, ORNL-1366, p. 10.

[4] W. J. Fretague, *Met. Div. Quar Prog. Rep July 31, 1952*, ORNL-1366, p. 10.

HRP METALLURGY

W. J. Fretague
E. C. Miller W. J. Leonard

SERVICE TO CORROSION AND ENGINEERING GROUPS

Examination of a sample holder of type 304 stainless steel has established the susceptibility of a sensitized, austenitic, stainless steel to intergranular corrosion attack in uranyl sulfate containing 100 g of uranium per liter at 100°C under crevice corrosion conditions that involved oxygen depletion of the solution.

A variety of samples of stainless steels have been prepared for the Static and Dynamic Corrosion Test groups in an effort to establish the effect of such metallurgical variables as mechanical working, heat treatment, and various descaling procedures.

Valve parts of titanium and special stainless steels have been subjected to hard-surfacing treatments, exposed to corrosion conditions in dynamic corrosion loops, and evaluated metallurgically. This work is continuing because completely satisfactory treatments have not been established.

WELDING OF TYPE 347 STAINLESS STEEL

Experimental work has been carried on in the welding of thick plates of type 347 stainless steel by using various combinations of passes, by using bare rod filler metal in the inert-gas shielded-arc method, and by using coated electrodes in the conventional, metal-arc welding method. Similar work has been done in the welding of type 347 stainless steel to a boiler grade of carbon steel. Tentative procedural specifications and a welder's qualification outline have been written for the heavy-section welding of type 347 stainless steel.

RADIATION DAMAGE STUDIES

Assistance has been given to the Solid State Division in the selection and preparation of impact specimens for exposure in the Oak Ridge graphite reactor and in the LITR. The materials prepared included several carbon steels, austenitic stainless steels, and titanium of various grades.

PROPERTIES OF TITANIUM

Vacuum-fusion analyses and impact tests have been performed on specimens of commercial-purity titanium, as well as on high-purity iodide titanium – as machined, as exposed to uranyl sulfate under static and under dynamic corrosion conditions, and after cathodical treatment – for the purpose of investigating the possibility of contamination and embrittlement by hydrogen during the course of reactor operation.

The limited results available to date are encouraging in that they do not indicate that uranyl sulfate corrosion adds any appreciable amount of hydrogen to commercial-purity titanium or that it becomes any more embrittled as a result of the corrosion. It should be remembered, however, that the tests are not sufficiently complete to be conclusive and that the commercial-purity titanium was rather brittle even before the efforts to introduce hydrogen.

FABRICATION

E. S. Bomar

HRE Recombiner. Operation of the HRE results in a continuous dissociation of the heavy-water moderator into deuterium and oxygen. One method of recombining these gases for return to the reactor makes use of a controlled catalytic reaction to reform heavy water. J. Ransohoff of the Reactor Experimental Engineering Division suggested the possibility of applying the catalyst to a metallic surface, which could serve as the high-temperature side of a heat exchanger. The need for a large reacting area led to the work described below.

The structure of metal built up by using a wire or powder spray gun is inherently porous and has a relatively rough finish. Since these properties provide increased surface area, it was decided to investigate the possibilities of these methods of fabrication. Experimental lengths of ¼-in.-OD tubing were prepared by spraying stainless steel on stainless steel tubing to a thickness of 0.010 inch. Bends of 180 deg caused separation of the sprayed layer from the tube. To minimize this, a thin layer of a brazing alloy was applied to the tube before spraying.

Approximately 0.005 in. of Nicrobraz alloy was applied to the tube by using a powder pistol. This

was covered with a 0.020-in. layer of type 302 stainless steel from a wire spray gun. The composite tube was then sintered at 1120°C in hydrogen. Since this sintering temperature is above the melting point of the Nicrobraz, a bond was created between the tube and the sprayed metal layer. The adherence during bending was much better than without the braze. Thirty tubes, ½ in. in outside diameter and approximately 10 to 12 in. long have been prepared for assembly into a small heat exchanger by the Reactor Experimental Engineering Division.

Riveting of Second HRE Impeller. A series of five rivets for a second titanium impeller were upset by using conditions established in assembling the first impeller.[1] The riveting proceeded without difficulty, and all rivets upset in a satisfactory manner, as indicated by a subsequent cleanup machining operation. All of the rivets were of the same length. The conditions for riveting are given in the following:

Rivet length, in.	1 3/64
Rivet distance, in.	0.178
Voltage on electrodes	4.20
Current, %	75
Approximate current, amp	1000
Time in cycles	50

[1] E. S. Bomar, *Met. Div. Quar. Prog Rep. July 31, 1952*, ORNL-1366, p. 18.

ANP METALLURGY

W. D. Manley

STATIC CORROSION

D. C. Vreeland E. E. Hoffman
L. D. Dyer

Fluoride Corrosion. Some concern had been expressed about the possibility of crevice corrosion in materials used to contain the molten fluorides. To check this possibility, tests were set up with specially prepared crevices. Ordinary static corrosion tubes were employed by partially crimping the lower section of the tube above the bottom weld so that a crevice about 1 in. long and approximately 1/16 in. wide was obtained. After being tested for 100 hr at 816°C with fluoride No. 14, the tubes were cut longitudinally through the partially crimped section and examined for evidence of accelerated corrosion. The crimped ends of several, ordinary, static-corrosion-test tubes were also examined for accelerated corrosion. Corrosion in these crevices appeared to be somewhat erratic, and some sections were unattacked. However, even in the sections that were attacked, the depth of penetration did not exceed that which normally would be expected for these materials after exposure to fluorides. Details of these tests are presented in Table 3.

TABLE 3. RESULTS OF EXAMINATION FOR ACCELERATED CREVICE CORROSION IN VARIOUS MATERIALS AFTER TESTING IN FLUORIDE NO. 14 FOR 100 hr AT 816°C

MATERIAL	METALLOGRAPHIC NOTES
Inconel (specially prepared crevice)	Subsurface voids to a maximum of 2 mils
Type 304 stainless steel (specially prepared crevice)	Subsurface voids to a maximum of 2 mils
Type 316 stainless steel (specially prepared crevice)	Subsurface voids to a maximum of 1 mil
Inconel (regular static test)	Subsurface voids to a maximum of 2½ mils
Type 304 stainless steel (regular static test)	Very little attack, a few subsurface voids to ½ mil
Type 309 stainless steel (regular static test)	Subsurface voids to a maximum of 1½ mils

A jig that can be used to put tapered crimps in tubing has been constructed and will be used in both static and seesaw crevice corrosion tests. By using this jig, a crevice $1\frac{3}{4}$ in. in length and varying in width from approximately 0.3 in. at the top to 0 in. at the bottom can be put in the test tubing. Thus if there is a critical dimension at which crevice corrosion will take place, it will be more likely to show up in one of these tapered crevices than in a crevice that is of the same width throughout its length.

The NACA whirligig rig is now in operation, and operational "bugs" are gradually being worked out. This device will make it possible to run relatively high-velocity corrosion tests with fluoride mixtures contained in Inconel and other suitable tubing. At the present time, a fluid velocity of approximately 10 fps is being employed.

Several Carboloy and Haynes Stellite alloys that may have possible ARE application as valve seat and facing materials have been subjected to static corrosion tests with the fluorides. Carboloys 44A and 55A were apparently unattacked in fluoride No. 27. The Stellites tested were attacked much more severely by fluoride No. 27 than by fluoride No. 14. These tests were run for 100 hr at 816°C in evacuated Inconel tubes. Figure 1 shows the type of attack occurring with the Stellites in the fluoride mixtures. The test results are presented in Table 4.

TABLE 4. RESULTS OF TESTS OF SEVERAL CARBOLOY AND HAYNES STELLITE ALLOYS IN FLUORIDE MIXTURES

Tests Conducted for 100 hr at 816°C in Inconel Tubes

MATERIAL	BATH	METALLOGRAPHIC NOTES
Carboloy 44A	Fluoride No. 27	No apparent attack
Carboloy 55A	Fluoride No. 27	No apparent attack
Carboloy 608	Fluoride No. 27	General roughening of surface, 1 to 2 mils
Carboloy 779	Fluoride No. 27	Some surface spalling to a depth of 1 mil, this may have occurred in grinding
Carboloy 907	Fluoride No. 27	Some surface spalling to a depth of 1 to 3 mils, this may have occurred in grinding
Haynes Stellite No. 3	Fluoride No. 14	Light attack of what appears to be a carbide phase, 1 mil in depth
Haynes Stellite No. 3	Fluoride No. 27	Selective attack of what appears to be a carbide phase, maximum depth 22 mils, minimum 12 mils, average 15 mils
Haynes Stellite No. 6	Fluoride No. 14	Selective attack of what appears to be a carbide phase, maximum depth 6 mils, minimum 2 mils, average 4 mils
Haynes Stellite No. 6 (specimen A)	Fluoride No. 27	Selective attack of what appears to be a carbide phase, maximum depth 24 mils, minimum 12 mils, average 15 mils
Haynes Stellite No. 6 (specimen B)	Fluoride No. 14	Selective attack of what appears to be a carbide phase, maximum depth 3 mils, minimum 1 mil, average 2 mils
Haynes Stellite No. 6 (specimen B)	Fluoride No. 27	Selective attack of what appears to be a carbide phase, maximum depth 29 mils, minimum 8 mils, average 11 mils
Haynes Stellite No. 19	Fluoride No. 14	Scattered attack to a depth of 2 mils
Haynes Stellite No. 19	Fluoride No. 27	Selective attack of what appears to be a carbide phase, maximum depth 29 mils, minimum 10 mils, average 20 mils

In previous tests with the fluoride mixtures plus small additions of magnesium, there had been some discrepancy in results, although the indications were that magnesium additions would not inhibit corrosion. Therefore tests were run with magnesium additions to both fluoride Nos. 14 and 27. Tests were also run with chromium additions to both these fluoride mixtures in order to confirm previous results. Confirmation was obtained; so there is indication that chromium does and magnesium does not inhibit corrosion in Inconel tubing. In the test of fluoride No. 14 with the magnesium addition, it was noted upon stripping that an extremely active, silvery, mushy metal was present in rather large quantities on the specimen, tube walls, and in the remaining fluoride. This metal had the appearance and all of the active qualities of NaK, such as burning and reacting vigorously with alcohol. It is believed that a reduction of some of the metal fluorides in the salt took place and liberated the elemental metals involved (sodium, lithium, potassium, and uranium). These tests were run for 100 hr at 816°C. Metallographic notes are listed in Table 5.

Fig. 1. Stellite No. 6 Tested in Fluoride No. 27 for 100 hr at 816°C. 250X

TABLE 5. RESULTS OF TESTS OF INCONEL IN FLUORIDE MIXTURES WITH CHROMIUM AND MAGNESIUM ADDITIONS FOR 100 hr AT 816°C

BATH	METALLOGRAPHIC NOTES
Fluoride No. 14 plus 5% Cr	No attack, but a thin layer (0.1 mil) of some material present, probably chromium
Fluoride No. 14 plus 5% Mg	Very heavy erratic attack on specimen, 1 to 10 mils deep; tube attacked heavily to a depth of 2 mils
Fluoride No. 27 plus 5% Cr	No attack on most of specimen; subsurface voids to 1 mil in a few places; no attack on tube, but a thin layer, which may be chromium, visible in some places
Fluoride No. 27 plus 5% Mg	A 2-mil layer of several phases appears to be present on the surface; ½ mil of subsurface voids beneath the layer

In some previous tests with fluoride No. 14 at high temperatures (1200 to 1300°C), it had been reported that there was no attack on Inconel because of the formation of a surface layer. It was thought that perhaps a pretreatment at high temperature would render Inconel immune to corrosion at the usual temperature of 816°C. Accordingly, two Inconel tubes were loaded with fluoride No. 14 and heated for 4 hr at 1250°C and then for 250 hr at 816°C. Light attack in the form of subsurface voids to a depth of 1 mil was noted in one tube, and ½ mil of similar attack was noted in the other tube.

Incoloy (32% Ni–21% Cr–47% Fe) was tested in fluoride No. 27 for 100 hr at 816°C. In a few places, subsurface voids to 2 mils could be noted. A photomicrograph of Incoloy after testing is shown in Fig. 2.

The descaling properties of fluoride No. 31 have been checked on oxidized Inconel at 816°C. As can be seen in Fig. 3, the oxidized Inconel was cleaned very well at all test times tried.

Liquid Metal Corrosion. Several tests have been run to determine the stability in sodium and NaK of the beryllium oxide to be used in the ARE moderator. Some tests have been conducted with full-size moderator blocks, whereas others were conducted with small samples (approximately ¼ by ¼ by 1 in.) of the same type of beryllium oxide. Three tests of full-size blocks in sodium and in NaK have been run. These tests were conducted in a type 347 stainless steel pot that was evacuated before the molten sodium or NaK was transferred to the pot by helium pressure. In test *a*, the beryllium oxide was in 255 in.^{3} of sodium for 213 hr at 816°C. Before transferring the sodium to the test pot, both sodium and pot were heated to approximately 250°C. No cracking or spalling of the beryllium oxide was noticeable immediately after test. The surface imperfections apparent in Fig. 4*a* occurred after the test specimen had been soaked in alcohol and water. The slight weight and dimensional changes noted after the test are listed in Table 6.

Test *c* was discontinued shortly after the NaK was transferred to the test container because of a leak in the apparatus. For this test, the NaK was transferred at room temperature to the hot container. The cracks visible in Fig. 4*c* may have been caused by this thermal shock. For test *b*, the NaK was transferred when both the NaK and the beryllium oxide were at room temperature. The test was run for 500 hr at 816°C with 255 in.^{3} of NaK. After testing, the beryllium oxide was badly

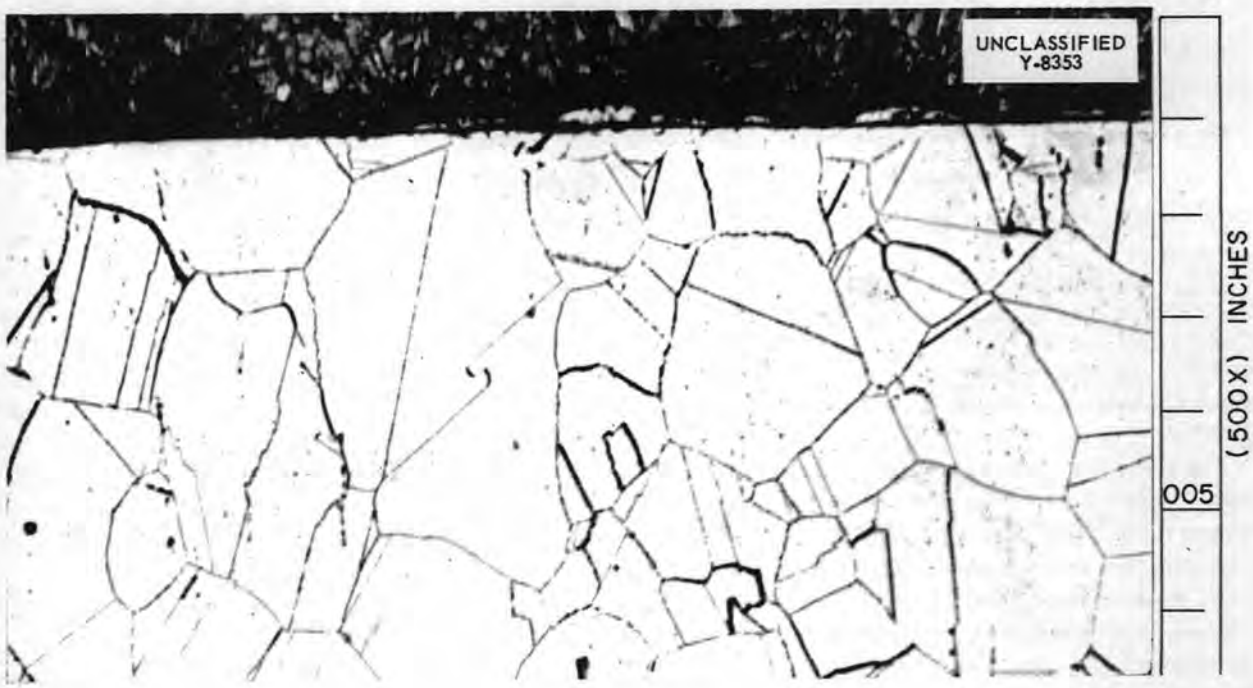

Fig. 2. Incoloy Tested in Fluoride No. 27 for 100 hr at 816°C. Etched with aqua regia. 500X

UNCLASSIFIED
Y-8348

Fig. 3. Oxidized Inconel Descaled by Fluoride No. 31 at 816°C.

TABLE 6. WEIGHT AND DIMENSIONAL CHANGES OF BERYLLIUM OXIDE TESTED IN SODIUM

	LENGTH (in.)	WIDTH (in.)	WEIGHT (g)
Before testing	5.914	3.706	3154
After testing	5.917	3.708	3221
Change (%)	+0.05	+0.05	+2.1
After cleaning in water and drying			3205
Change (%)			+1.6

TABLE 7. WEIGHT AND DIMENSIONAL CHANGES OF BERYLLIUM OXIDE TESTED IN NaK

	LENGTH (in.)	WIDTH (in.)	WEIGHT (g)
Before testing	5.909	3.714	3160
After testing	5.899	3.712	3205
Change (%)	–0.17	–0.05	+1.4
After cleaning in water and drying			3187
Change (%)			+0.85

cracked, as can be seen in Fig. 4*b*. The weight and dimensional changes noted are listed in Table 7.

The small beryllium oxide specimens were run in NaK in the rocker furnace for 100 hours. Hot-zone temperatures were approximately 830°C; cold-zone temperatures were approximately 450°C. Specimens were crimped into the hot end of the tube to prevent their sliding from the hot to the cold end. Specimens indicated as "low density" had a density of approximately 2.3; those indicated as "high density" had a density of approximately 2.8. Specimens indicated as "dehydrated" were dried for 24 hr at 125°C before testing. Information derived from these experiments consists of weight change data and results of analysis of the NaK for BeO after testing. Except for one test, the amount of beryllium oxide lost by weight change failed to match the amount of beryllium oxide found by analysis of the NaK. However, the same conclusion can be drawn from both weight loss and analysis data; that is, in these tests the low-density beryllium oxide was less stable than the high-density beryllium oxide. When the NaK was filtered after the

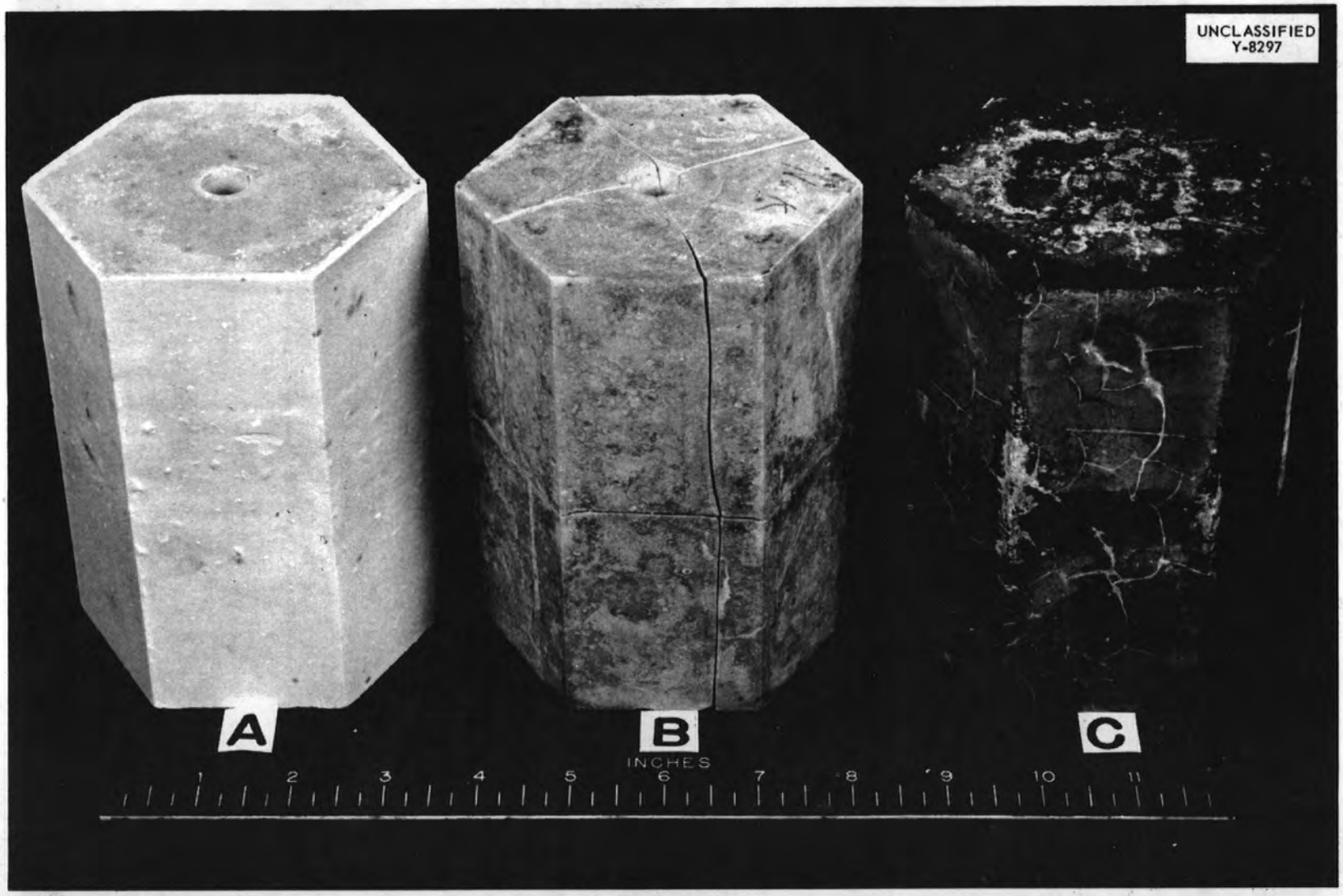

Fig. 4. Beryllium Oxide Moderator Blocks After Testing in Na or NaK. (*a*) Tested in Na. (*b*) Tested in NaK. (*c*) Tested in NaK.

test and analyzed for beryllium oxide, 3 to 4 ppm was found. The rest of the beryllium oxide detected by analysis was found on the filter, in washings from the test tubing, etc. After stripping in alcohol, there was some slight evidence of cracking in the high-density specimens and some slight evidence of spalling in the low-density specimens. Weight change and analysis data are given in Table 8.

A series of seesaw tests of sodium-lead mixtures have been run in Inconel and types 430 and 304 stainless steel tubing for 100 hours. The lead for these tests was purified by bubbling hydrogen through molten lead at 750°C for 1½ hours. All Inconel tubes were attacked in the hot zone. The severity of attack decreased with increasing sodium additions, but the attack was still appreciable with a 30 wt % sodium addition. Figures 5 and 6

TABLE 8. WEIGHT CHANGE AND ANALYSIS DATA FOR BERYLLIUM OXIDE SPECIMENS TESTED IN NaK

BERYLLIUM OXIDE SPECIMEN	WEIGHT LOSS ($g/in.^2$)	WEIGHT LOSS (%)	TOTAL WEIGHT LOSS (mg)	TOTAL BeO FOUND BY ANALYSIS (mg)
Low-density, as-received*	0.0454	2.38	30.7	14.26
High-density, as-received	0.0286	1.25	18.9	4.97
Low-density, dehydrated	0.0893	5.15	47.0	9.91
High-density, dehydrated	0.0104	0.52	6.1	6.02

*Test run for only 16 hr, other tests were run for 100 hours.

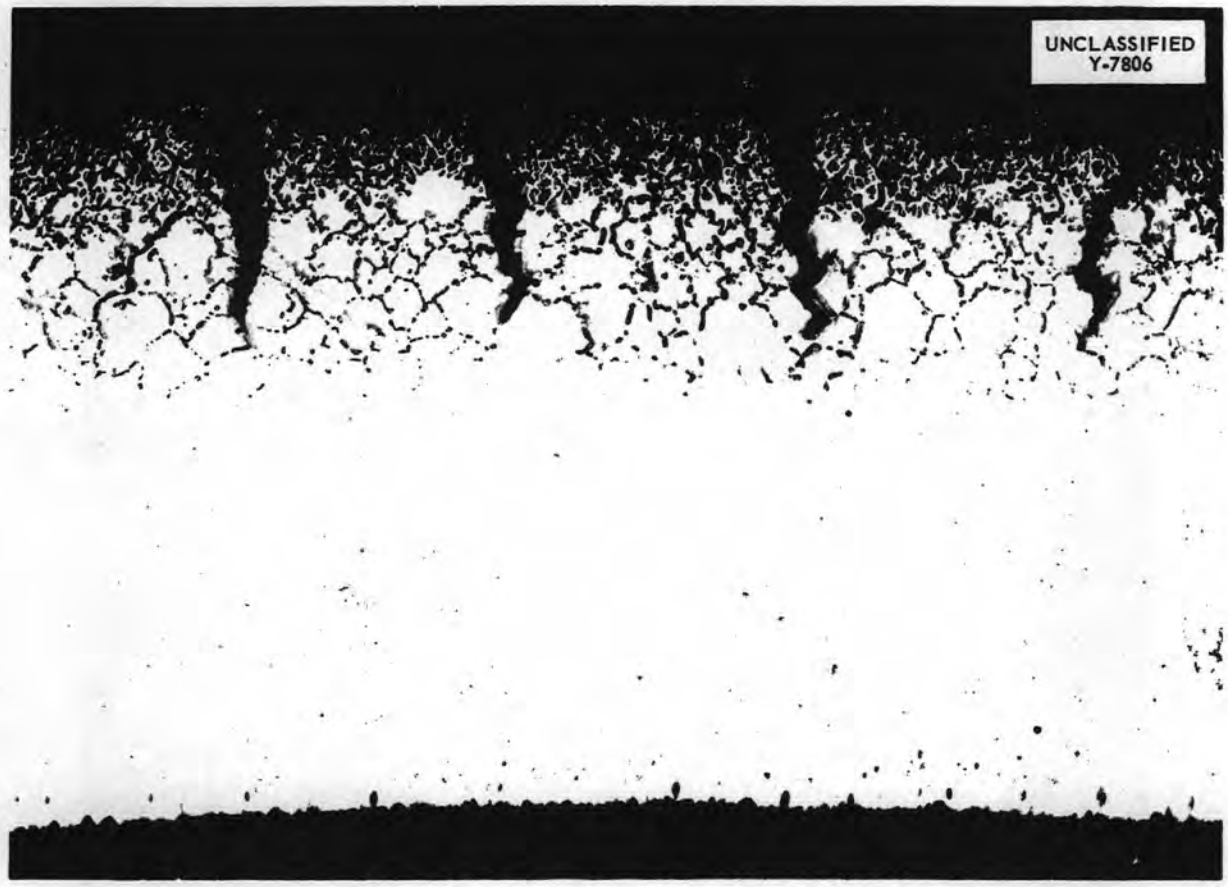

Fig. 5. Inconel After a Seesaw Test in 15% Na–85% Pb Alloy. Unetched. 100X

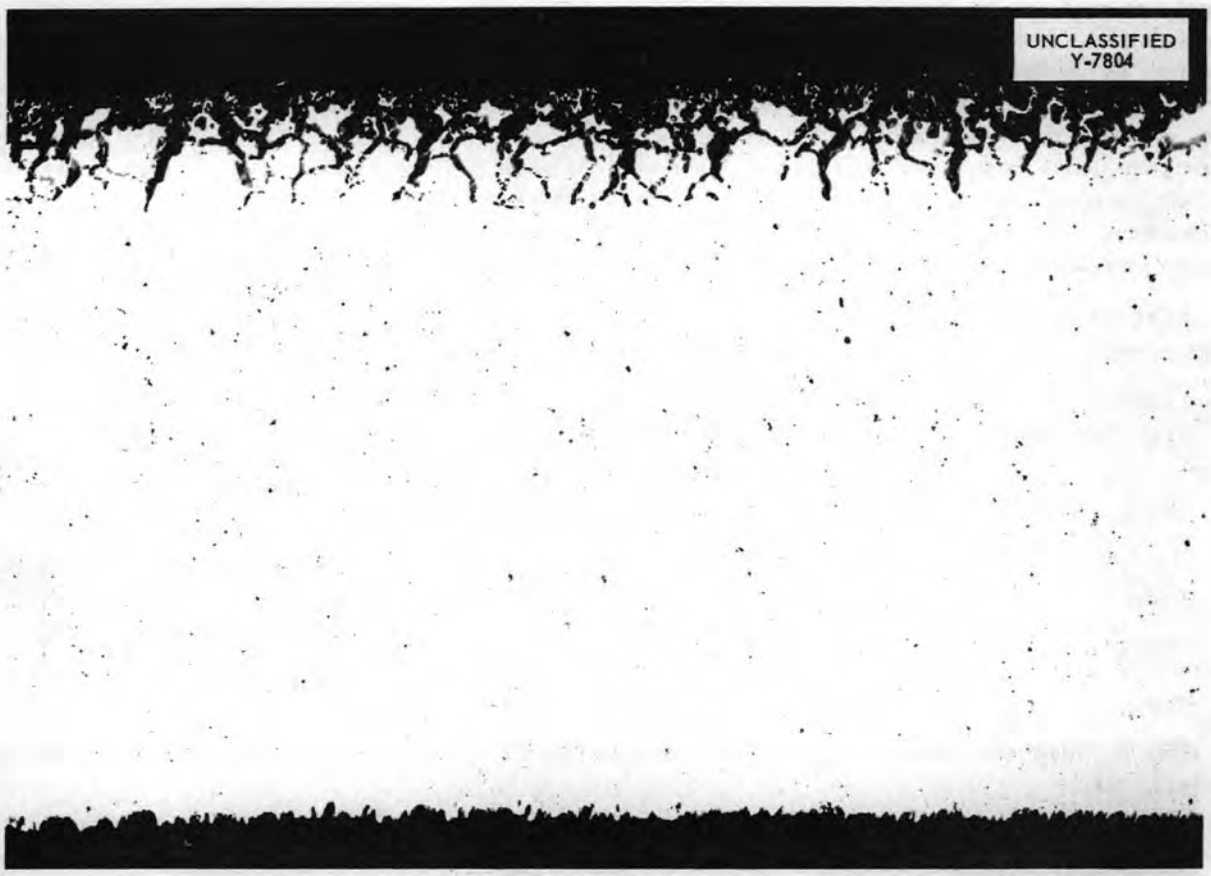

Fig. 6. Inconel After a Seesaw Test in 30% Na–70% Pb Alloy.

show the type and extent of attack of two of these sodium-lead mixtures. In no case was attack or deposition of crystals noted in the cold zone upon metallographic examination; however, in several of the tubes, crystals could be detected in the bath material. In the test with type 430 stainless steel tubing, there was very little corrosive effect by the sodium-lead mixtures. Apparently type 430 stainless steel is resistant to attack under the conditions of these tests. Figure 7 demonstrates how well this material stood up during these tests. Type 304 stainless steel also showed good resistance to these corrodants. Figure 8 shows a section of the hot zone of a tube after exposure to 5% Na-95% Pb alloy. There was essentially no attack in any of the tests with type 304 stainless steel. A summary of these tests is given in Table 9.

Two-component static tests of several materials were run with lithium at 1000°C to furnish a basis of comparison with three-component tests run in the past. Much more severe attack was noted in the three-component tests, 10 to 15 mils penetration being quite common, than in the two-component tests. It should be emphasized, however, that these most recent tests were static tests and that more severe attack might result in dynamic systems. Results of these tests are presented in Table 10.

Incoloy (32% Ni–21% Cr–47% Fe) was tested for 100 hr at 816°C in sodium, lithium, and lead. No attack was noted in either sodium or lithium, but some crystal deposition was apparent in the test with lithium. In the test with lead, 1 to 2 mils of intergranular penetration could be noted.

DYNAMIC CORROSION

G. M. Adamson

Zirconium Fluoride Base Fuels. The attack found in Inconel loops in which fuzrna No. 27 has been circulated has doubled since the material has been produced in the pilot plant. Studies have been

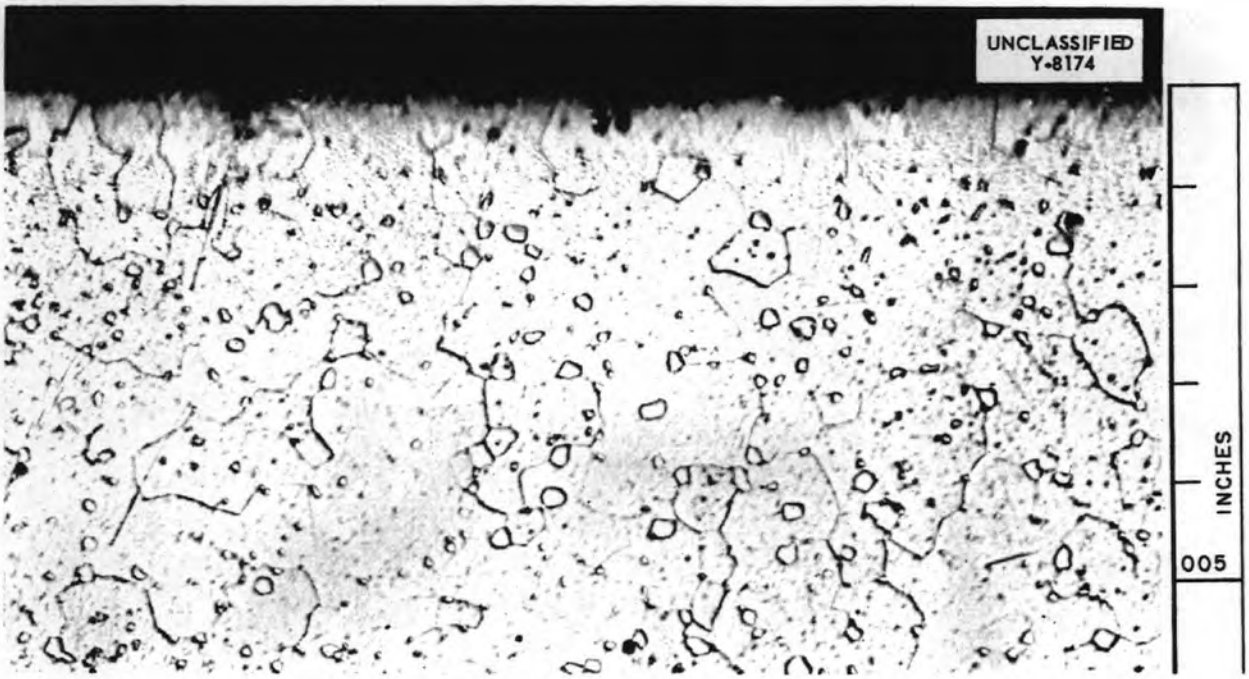

Fig. 7. Type 430 Stainless Steel After a Seesaw Test in 5% Na–95% Pb Alloy. Etched with aqua regia. 500X

Fig. 8. Type 304 Stainless Steel After a Seesaw Test in 5% Na–95% Pb Alloy. Hot zone at 830°C. Etched with aqua regia. 250X

TABLE 9. SEESAW TESTS OF VARIOUS MATERIALS IN SODIUM-LEAD MIXTURES FOR 100 HOURS

MATERIAL	BATH	AVERAGE TEMPERATURE (°C)		METALLOGRAPHIC NOTES
		Cold Zone	Hot Zone	
Inconel	5% Na–95% Pb	530	820	Terminated after 18 hr – no circulation, 12 mils of intergranular attack in hot zone
	10% Na–90% Pb	330	870	Intergranular attack entirely through 35-mil wall in hot zone
	15% Na–85% Pb	315	860	Heavy intergranular attack in hot zone to depth of 15 mils
	20% Na–80% Pb	395	855	Intergranular attack in hot zone to depth of 12 mils
	25% Na–75% Pb	470	850	Intergranular attack in hot zone to depth of 5 mils
	30% Na–70% Pb	485	850	Intergranular attack in hot zone to depth of 6 mils
Type 304 stainless steel	5% Na–95% Pb	560	830	Essentially no attack in either hot or cold zone
	10% Na–90% Pb	575	840	Essentially no attack in either hot or cold zone
	15% Na–85% Pb	545	830	Essentially no attack in either hot or cold zone
	20% Na–80% Pb	585	825	Essentially no attack in either hot or cold zone
	100% Pb	565	830	Intergranular attack in hot leg to depth of 1 to 2 mils
	25% Na–75% Pb	600	835	Essentially no attack in either hot or cold zone
	30% Na–70% Pb	600	835	Essentially no attack in either hot or cold zone
Type 430 stainless steel	5% Na–95% Pb	565	850	Essentially no attack in either hot or cold zone
	10% Na–90% Pb	580	845	Essentially no attack in either hot or cold zone
	15% Na–85% Pb	575	820	Essentially no attack in either hot or cold zone
	20% Na–80% Pb	575	810	Essentially no attack in either hot or cold zone
	25% Na–75% Pb	550	805	Essentially no attack in either hot or cold zone
	30% Na–70% Pb	610	835	Essentially no attack in either hot or cold zone

made to determine whether the larger batch size and insufficient over-all treatment times or the presence of nickel, iron, and hydrogen fluorides was the cause of the increased attack. When fulinak No. 14 was prepared by the same method as that used for the preparation of fuzrna No. 27, an increase in attack was also found. Table 11 is a summary of the corrosion results for the Inconel loops in which these fuels have been circulated. The results for the first seven loops listed were reported previously but are presented again for comparison. The last three loops are the new ones that show the increase in attack. Although some of the original loops show a fair amount of attack, that attack could be attributed to the cleaning cycle. It has been shown, both with other fluorides[1]

[1] G. M. Adamson, *Met. Div. Quar. Prog. Rep. Oct. 31, 1952*, ORNL-1437, p. 21.

and with lead, that the cleaning methods used caused an increase in attack. When cleaning is responsible, a different type of attack is found than when the fluorides themselves are the cause. The attack found in the new loops (239, 244, and 245) should be comparable to the attack found in loop 234. The new attack is actually as deep or deeper than that found in all the previous loops, even with the cleaning variables included. One other difference in these two sets of loops is that

TABLE 10. RESULTS OF TWO-COMPONENT STATIC TESTS WITH LITHUM AT 1000°C

MATERIAL	TIME OF TEST (hr)	METALLOGRAPHIC NOTES
Type 316 stainless steel	100	No sign of attack on sections exposed to liquid phase, 2½ mils of intergranular attack on sections exposed to vapor phase
Inconel	100	Some mass transfer crystals could be noted on the surface, no attack in vapor zone, 3 to 4 mils of subsurface voids on tube in bath zone
Type 304 stainless steel	400	Intergranular penetration to depth of 1 to 2 mils, and transformation from austenite to ferrite

TABLE 11. CORROSION OF INCONEL LOOPS CIRCULATING ZIRCONIUM FLUORIDE BASE FUELS

LOOP NO.	FUEL NO.	CONDITIONS	HOT LEG CORROSION
226	Funazrk 26	H_2 cleaned	General pitting, 1 mil, widely scattered intergranular pitting, average 7 mils, maximum 10 mils, large voids in grain boundaries
221	Funazrk 21	Degreased	Light to moderate intergranular and general pitting, 3 mils to maximum of 7 mils, no large voids
228	Funazrk 21	H_2 cleaned	General pitting, about 3 mils, scattered intergranular attack, up to maximum of 13 mils, large voids in boundaries
234	Fuzrna 27	Degreased	General pitting, 2 mils, with lightly scattered intergranular attack, up to maximum of 5 mils, small voids
236	Fuzrna 27	H_2 cleaned	General pitting, up to 2 mils, moderate intergranular attack, up to maximum of 10 mils, average 8 mils, large voids in boundaries
231	Fuzrna 27	NaK cleaned	Moderate general pitting, up to 9 mils, no large voids
237	Fuzrna 30	Na cleaned	General pitting, up to maximum of 7 mils, average 4 mils, no large voids
239	Fuzrna 27	Degreased, sample inserted	Moderate to heavy general and intergranular attack, 9 to 17 mils, few medium size voids, rest small
244	Fuzrna 27	Degreased	Moderate general and intergranular attack, up to maximum of 9 mils, average 5 mils, no large voids
245	Fuzrna 27	Degreased	Moderate to heavy general and intergranular attack, maximum of 12 mils, average 7 mils

an as yet unidentified brown material was found in the fluorides in the new loops but not in the previous loops.

Batch Size. The most apparent difference in the operation of these two sets of loops is that the previous loops were filled from small batches made in the laboratory, whereas the new loops were filled from 50-lb batches made in a semiproduction operation. Since the attack now being measured is comparable to that normally found with fulinak No. 14, the amount of the attack is not serious, but the trend toward increasing amounts may be serious. In the final production operation, 250-lb batches instead of the present 50-lb batches will be manufactured.

A series of loops was run to determine whether the increase in batch size was responsible for the increase in attack. Loops were run in 100-and 500-hr tests with fuels prepared in 5-lb batches and in 50-lb batches. Extreme care was used to avoid any chance of contamination during the handling of these batches. Two days were required for each filling operation. The results from these runs are tabulated in Table 12. With both 100- and 500-hr operation, more corrosion was measured from the small batches than from the large ones. The increase in batch size was not the reason for the increase in attack. Since in these loops the attack is still extensive, poor handling during filling is also eliminated as the cause.

Retreatment. Two small batches of fuzrna No. 27 were taken from the 50-lb batch used for the batch size tests and then given a complete retreatment. The results obtained by circulating these retreated batches in Inconel are listed in Table 13, along with the results from loop 261 in which fuzrna No. 30 had been circulated. The batch of fuzrna No. 30 had received an additional hydrogen purge. Lower corrosion rates were obtained for loops 261 and 267, but the attack for loop 268 was deeper than the average depth. The only conclusion is that some major variable still has not been controlled.

During the filling of the loops for both of the batch size and retreatment tests, the operators reported the presence of hydrogen fluoride in the purging gases. The Chemistry Division is now studying the final purging operation to assure that all hydrogen fluoride is removed. Static tests have shown that both nickel and iron fluorides are very harmful. Both of these materials can be formed

TABLE 12. RESULTS FROM LOOPS RUN TO DETERMINE EFFECT OF BATCH SIZE

LOOP NO.	BATCH SIZE (lb)	HOURS OF OPERATION	ATTACK (mils)		CORROSION INTENSITY
			Maximum	Average	
265	5	100	5	3	Light to moderate
263	50	100	4	2	Light to moderate
266	5	500	15	10	Moderate
264	50	500	8	6	Heavy to moderate

TABLE 13. RESULTS FROM LOOPS RUN WITH RETREATED BATCHES

LOOP NO.	HOURS OF OPERATION	ATTACK (mils)		CORROSION INTENSITY
		Maximum	Average	
267	100	3	1	Moderate
268	500	13	10	Moderate
261	500	5	3	Moderate

during the hydrogen fluoride treatment, and therefore their elimination is also receiving considerable study.

Hydrofluorinated Fulinak No. 14. One other series of tests points to poor purification technique as the cause of the increased corrosion. The attack found in Inconel loops in which fuzrna No. 27 was circulated was much less than had been found in the loops in which fulinak No. 14 was circulated. Since the fuzrna No. 27 had been "purified" with hydrogen and hydrogen fluoride, its higher purity appeared to be a logical explanation for the decreased attack. Two special batches of fulinak No. 14 were therefore prepared by the group that makes the fuzrna No. 27, and the techniques for preparing fuzrna No. 27 were used. These batches produced attack on Inconel that was even deeper than normal. In loop 249, the maximum attack was 30 mils and the average was 20 mils, in loop 256 the maximum was 18 mils and the average was 10 mils. The first analyses of the two batches of fulinak No. 14 that went into these loops showed very high values of iron, chromium, and nickel. The heel from the second batch was resampled after the loop had been filled and showed much lower, but still high, values for chromium and iron and a very high nickel content. Because of these discrepancies, two additional batches were prepared. The loops in which these batches were circulated have been sectioned, but neither the metallographic nor chemical results are available. In both loops, metallic crystals were found in the hot leg and in the trap. The operators again noted the presence of hydrogen fluoride during the filling operation.

Additives to Fluorides. Various additions have been made to the fluorides in an attempt to decrease attack on the loops. Zirconium and titanium hydrides have been tested as additives, and various metal additions, such as chromium, iron, and nickel, have been tried.

Hydrides. The fact that zirconium hydride will reduce the attack in the fuzrna No. 27–Inconel system has been confirmed. The addition of ½% zirconium hydride to loop 248 reduced the depth of attack to between 1 and 4 mils. This is lower than normal attack, but it is deeper than that found when zirconium hydride is added to fulinak No. 14. The fluoride underwent considerable transformation, as evidenced by the presence of a brown material. These results confirmed those reported previously for loop 243.

Fulinak No. 14 plus ½% titanium hydride was circulated in Inconel, and the maximum penetration measured was 2.5 mils. This attack is much less than that in the standard loops, but it is not quite so low as was obtained when zirconium hydride was added. Surface layers were found in both the hot and cold legs. These layers must receive additional study if hydrides are to be used as inhibitors.

Metals. The three most common impurities found in the fuel are nickel, iron, and chromium. One loop in which chromium metal powder had been added to fulinak No. 14 was discussed in the previous report.[1] This test was repeated and, again, no change in depth of attack was found. No unusual layers were found, and the chromium content of the fluorides from the loop was normal, so again the chromium metal did not go into solution. Chromium metal powder was then added to a transfer pot before the fluorides were placed in it. After the fluorides had been added, the pot was kept hot and helium was blown through it for 30 minutes. Again, average attack was found after this material had been circulated in Inconel. Although the chemical results are not yet available, it seems that the chromium did not go into solution. Why it dissolves so easily from the loop walls but does not dissolve from a metal powder is still to be determined.

As another approach to this problem, a section of Inconel pipe was chromium plated and welded into the hot leg of a loop. After fulinak No. 14 had been circulated, the depth of attack was the same in adjacent plated and unplated sections. No traces of the chromium plate remained on the walls. A deposited layer was found in the cold leg, and the chromium concentration in the fluorides was higher than normal.

One Inconel loop was operated with fulinak No. 14 to which had been added ½% of both metallic iron and nickel. The hot leg attack in this loop measured 15 mils, which is an average figure. This shows that the presence of metallic iron or nickel is not harmful. The effects of their compounds will be checked in seesaw tests before these additions are tried in other loops.

Inserted Corrosion Samples. Two Inconel loops were operated with small, flat Inconel samples inserted in the top of the hot leg. Loop 239 circulated fuzrna No. 27 and loop 240 circulated fulinak

No. 14. In loop 239, the wall attack in the hot leg consisted of moderate intergranular and general attack from 9 to 17 mils deep. The sample in this loop was attacked to a depth of only 1 mil. Loop 240 showed moderate wall attack of 5 to 11 mils, whereas the inserted samples had light attack, up to 3 mils in depth. Two more loops were then circulated with small, thin-walled tubes inserted in the hot leg. Thermocouples inserted in these tubes show that a large temperature drop is not responsible for the lack of attack on the samples. In the loop circulating fulinak No. 14, the thermocouple inserted in the sample read 15°F lower than the standard, hot-leg thermocouple, whereas the reading on the thermocouple inserted in the loop circulating fuzrna No. 27 was only 10°F lower. The standard hot-leg temperature is measured at the top of the leg at a position about 1½ in. above the heaters. Since a thermal driving force is necessary, the wall opposite a heater may be hotter than the measured temperature. This would cause a drop slightly larger than measured here, but it seems unlikely that it would be greater than 50°F. The results from these loops checked with the results from those with the flat samples in that with both fluoride No. 14 and fluoride No. 27 the wall attack was normal, however, the inserted tubes were attacked to only 1 mil. With fuzrna No. 27 the cold leg insert also showed an attack of 1 mil, but no attack was found with fulinak No. 14.

Crevice Corrosion. One more loop has been operated in the study of crevice corrosion.[1] The new study was made with an Inconel loop with two crevices built into the hot leg, fuzrna No. 27 was the circulated fuel. The upper hot-leg section showed a maximum attack of 16 mils and an average of 12 mils, whereas the lower hot-leg section had a maximum attack of 9 mils. The maximum attack in the crevices was 19 mils and the average was 12 mils. The intensity of attack in the crevice was several times that in the straight section. This confirms the results obtained when fulinak No. 14 was circulated in that the attack is slightly deeper but the intensity of attack has been greatly increased.

Temperature Variations. A type 316 stainless steel loop circulated 500 hr with fulinak No. 14 without signs of plugging by keeping the minimum cold-leg temperature above 1500°F. This was the first stainless steel loop to operate 500 hr with fulinak No. 14. At the end of 500 hr, the temperatures were lowered and the loop was allowed to circulate in a normal manner. It then plugged after an additional 366 hours. The hot leg was found to be very rough, and there was heavy intergranular attack to a depth of 6 mils. It is quite possible that some even removal had taken place. A metallic layer was found in the cold leg.

Miscellaneous Loops. Inconel loop 246 circulated zrnaf No. 32[2] (fuel No. 30 without uranium) for 500 hr at 1500°F. Scattered intergranular attack of from 3 to 8 mils was found in the top section of the hot leg. The lower section showed general pitting to a depth of 1 mil, with an occasional patch up to 6 mils in depth. No deposit was found in the cold leg. This attack is deeper than that found with previous fluorides that did not contain uranium.

One Inconel loop circulated 500 hr with benaf No. 35.[3] The maximum hot leg attack was 9 mils and the average was 4 mils. There was more concentrating of the voids in the grain boundaries than is normally found, and the voids were larger. A nonmetallic deposit was found in the cold leg. The attack mechanism of both these coolants seems to be the same as that for the other fluorides.

WELDING

P. Patriarca G. M. Slaughter

Cone-Arc Welding. The recent fuel-to-NaK heat exchangers for reactor research have been designed to include small, Inconel, tube-to-header subassemblies. After these pressure-tight subassemblies are fabricated, they can then be welded into one larger test assembly. It can be seen that the large number of tube-to-header joints to be heliarc welded would make a semiautomatic method for welding extremely desirable.

Therefore the cone-arc welding technique was applied to preliminary experiments in this subassembly fabrication. Since the heat exchanger is to be operated at a moderately high pressure for the temperature involved, dished header sheets are desirable. If the plane of the bottom of the header is kept level during welding, it is obvious that unequal arc distances will prevail around the periphery of many of the tubes. Thus the ability

(2) Composition 52 mole % NaF, 48 mole % ZrF_4.
(3) Composition 57 mole % NaF, 43 mole % BeF_2.

to make consistently sound welds on the dished header depends to a large degree upon the selection of conditions that will minimize these variations in arc distance. Offsetting the tungsten electrode from the center of the tube prior to welding and the use of a ball-and-socket joint arrangement from which the header can be pivoted are obvious means of equalizing the arc distance around the tube periphery.

Preliminary experiments on this problem have consisted of the investigation of the variables of arc current, arc time, and electrode distance required to produce consistently leak-tight welds. Figure 9, which is a photograph of an experimental test specimen after cone-arc welding, illustrates the tendency for uneven melting around some of the tube peripheries when the tungsten electrode is centered over the tube with the header plate axis perpendicular to the electrode axis. The diameter of the header plate is $2\frac{1}{4}$ in. and the plate thickness is 0.125 inch. The tubing has an outside diameter of 0.148 in. and a 0.025 in. wall; the hole center-to-center distance is approximately 0.378 inch.

Fig. 9. An Experimental Heat Exchanger Subassembly After Cone-Arc Welding. Uneven melting occurred around some of the tube peripheries when the tungsten electrode was centered over the tube.

Some difficulties have been encountered with joints that are not pressure-tight, but it is expected that further experiments will enable the production of subassemblies that will be completely sound. In each test assembly that has been fabricated so far, only one or two joints were unsatisfactory, the others being pressure-tight to air at approximately 60 psig. This indicates that an improvement in technique or a slight variation in welding conditions should help to improve the quality of these cone-arc welded joints.

Resistance Welding. A study was made of the electric-resistance spot welding of stainless steel clad fuel elements, and an investigation is being made of the feasibility of spot welding cold-rolled thorium sheet.

Spot Welding of Clad Fuel Elements. A study was made of the electric-resistance spot welding of stainless steel clad fuel elements with a total fuel element thickness of 0.030 in. and a core composition of 50% UO_2 (–325 mesh) and 50% Fe (–325 mesh). Satisfactory spot welds were considered to be those that exhibited good penetration and were nonporous and crack-free. Core damage resulting from thermal cracking or other welding factors should not be evident in a satisfactory joint.

Under the conditions of electrode force and weld time that were found to be optimum from the experiments conducted, it was found that the current range within which metallographically suitable welds can be produced is approximately 200 amp, or 3% of the optimum value. This current range is extremely narrow when compared with the range for most production resistance welding. Minor variations in sheet contact resistance, line voltage, and other resistance welding variables could easily result in the need for a wider current range.

An example of core damage resulting from the use of a slightly excessive welding current is shown in Fig. 10. Although excellent penetration was obtained, the presence of dark areas in each core is evident. Since this defect was thought to arise from very slight expulsion of molten metal, the optimum value of current recommended for this thickness of material is slightly less than the current used in producing this weld.

Other core compositions will be investigated in further experiments in an attempt to find materials that will permit the use of a wider welding-current

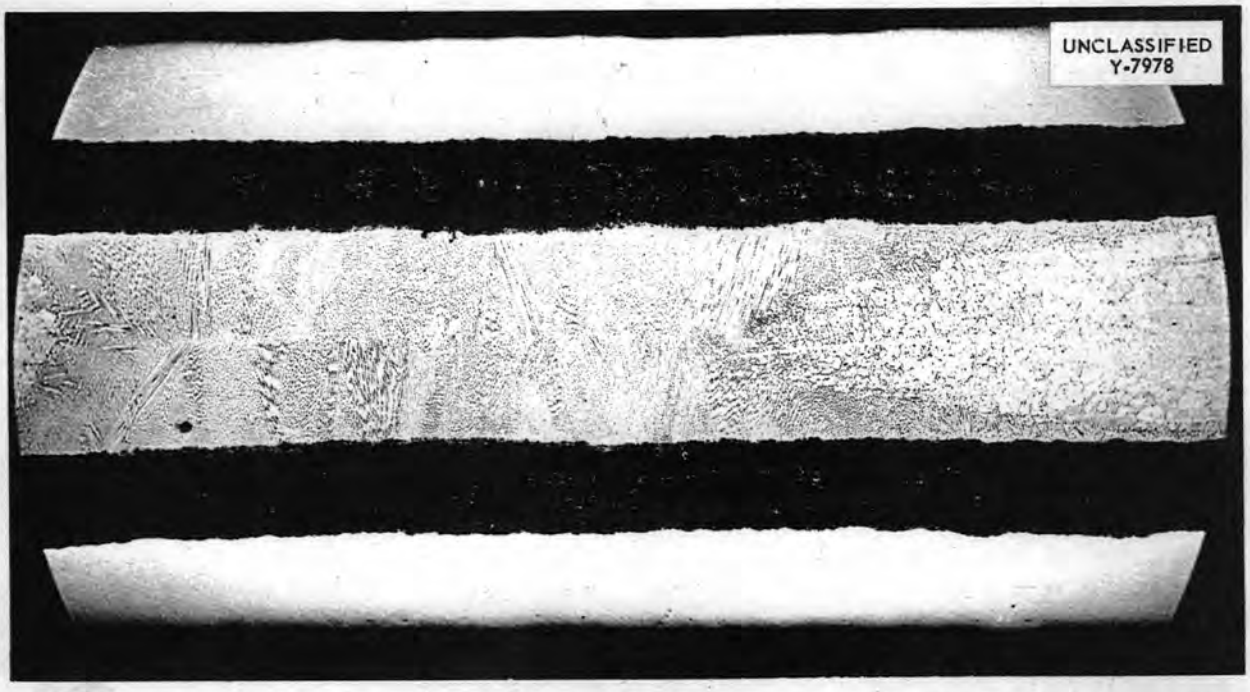

Fig. 10. A Spot Weld Made at a Welding Current of 6300 Amperes. Excellent weld penetration present; however, core damage rather severe, as evidenced by the dark areas. Etched with aqua regia. 50X

range. The use of stainless steel as a substitute for iron, or the use of a higher metal-to-UO_2 ratio, might aid in widening the current range.

Spot Welding of Thorium. A short investigation is being conducted on the feasibility of spot welding cold-rolled thorium sheet with a conventional single-phase press-type spot welder. The optimum value of electrode force for 0.025-in. thorium sheet was determined and welds have been made over a wide range of current. Although metallographic work on these samples has not been completed, it is hoped that it will give an indication of the permissible range of current over which satisfactory welds can be made.

Three tensile-shear lap welds were also made at each of these values of welding current, and the corresponding shear-strength vs. welding-current curve is shown in Fig. 11. The graph was plotted to show the scatter of shear-strength data, and the maximum, minimum, and average strengths of the three tests are shown for each current. The curve is very similar to that expected from a material such as low-carbon steel. Shear strengths increase with welding current up to a certain point and then level off. Also, as is usually the case,

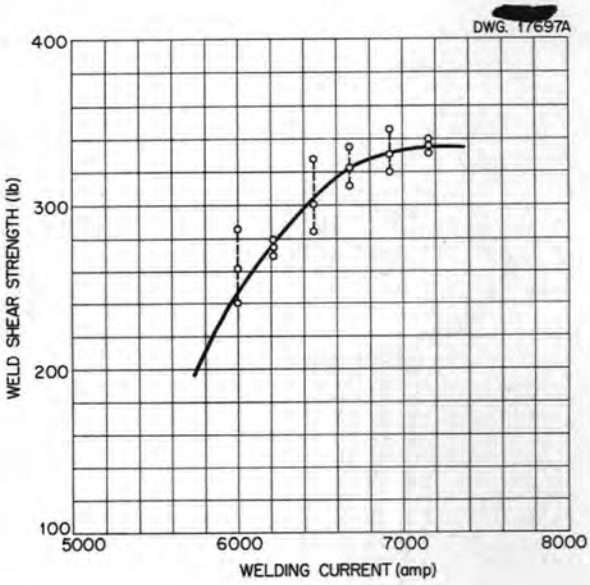

Fig. 11. Characteristic Curve of Shear Strength vs. Current for Thorium Spot Welds, Showing Maximum, Minimum, and Average Values of Three Tests.

the scatter is greater at lower values of shear strength. The actual maximum values of shear strength are approximately the same for thorium as for low-carbon steel. Since the ultimate tensile strengths of the two materials are similar in magnitude, this similarity of the maximum shear strengths would be expected if complicating factors such as cracking, porosity, or brittleness in the heat-affected zone were not present.

Figure 12 shows a thorium spot weld at 6900 amperes, which corresponds to an optimum value from the strength-current curve. It can be seen that an excellent degree of bonding is present. Figure 13 shows the characteristic appearance of lower-strength thorium spot welds. This weld was made at 6000 amperes. A faint trace of the original sheet-to-sheet interface can still be seen.

Fabrication of Heat Exchanger Test Units. It is necessary to develop techniques for successfully brazing large, complicated heat exchanger test assemblies of the type of interest to ANP, and two actual units have been assembled and subjected to the Nicrobrazing operation. Figure 14 shows the first heat exchanger after brazing in dry hydrogen by canning techniques. As can be seen from the photograph, the fins are badly warped and distorted, and in some cases they are even brazed together. After leak testing with helium, it was found that there were leaks in the tube-to-fin matrix, as well as in the tube-to-header joints of the manifold section. The tube-to-header joints could be repaired by rebrazing, but the many leaks in the body of the unit are almost impossible to repair successfully.

Examination of the completed unit revealed several factors that probably were important in causing the leaks and excessive distortion and also suggested techniques to overcome these flaws

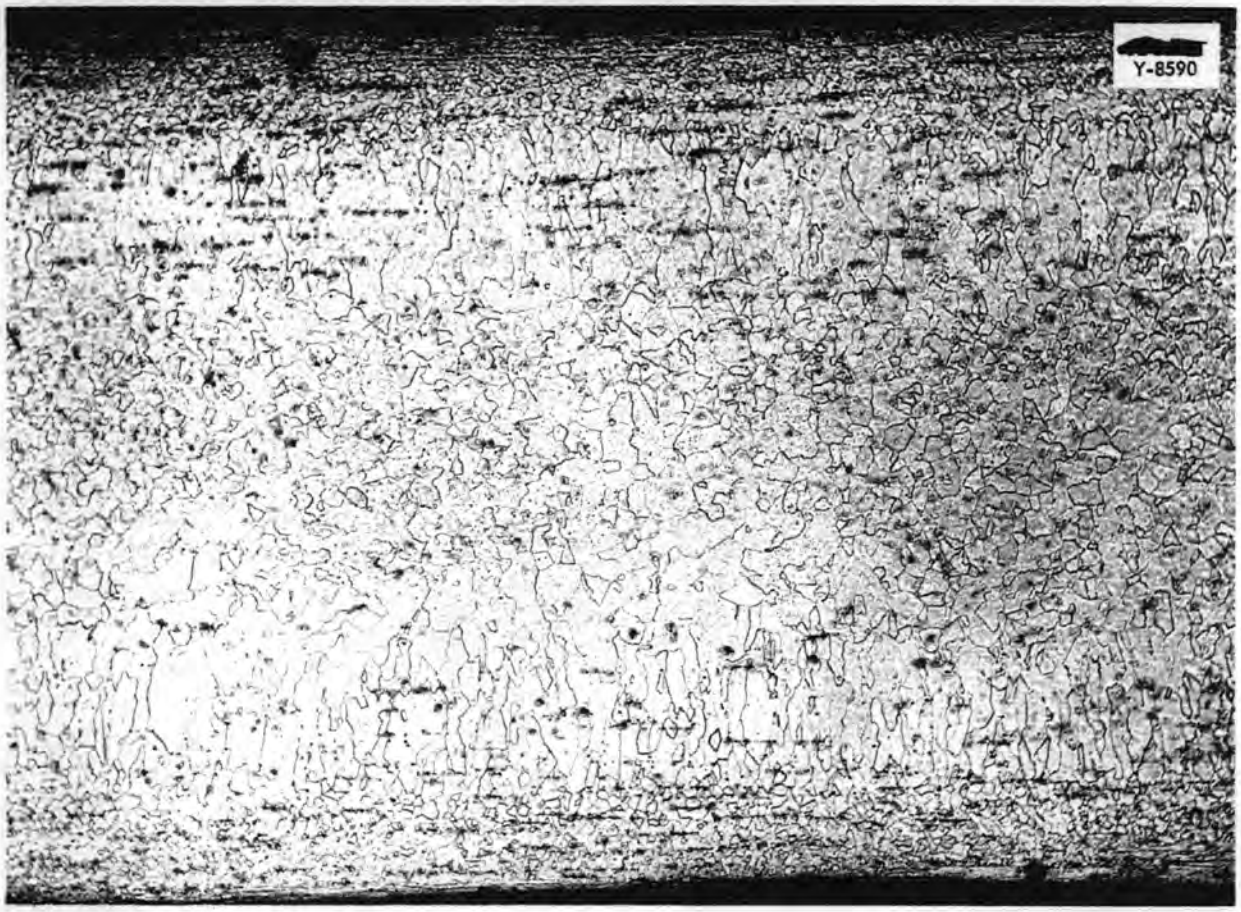

Fig. 12. Thorium Spot Weld Made at 6900 Amperes. High degree of welding occurred. Electrolytically etched with $HClO_4 + C_2H_5OH$. 100X

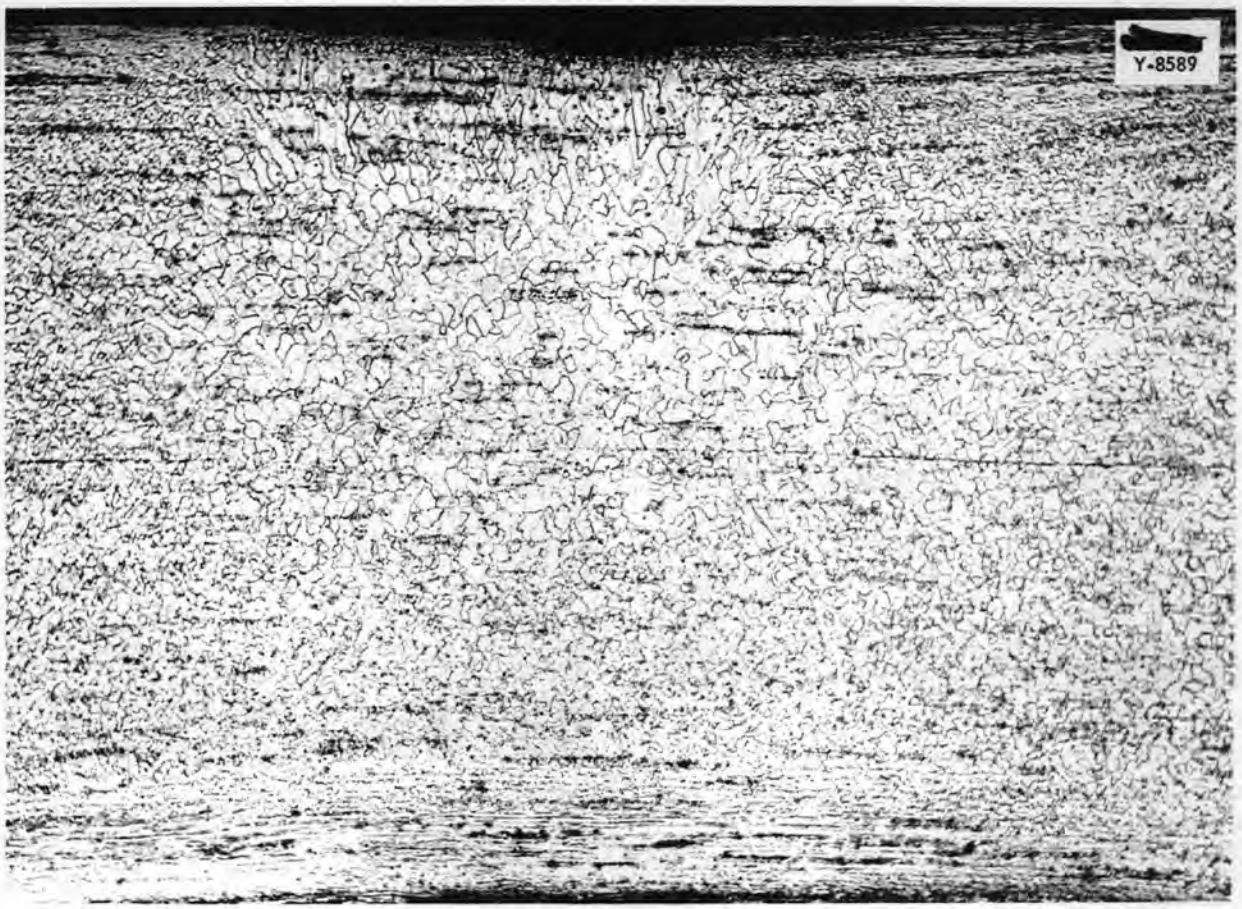

Fig. 13. Thorium Spot Weld Made at 6000 Amperes. Slight recrystallization across sheet-to-sheet interface present. Electrolytically etched with $HClO_4 + C_2H_5OH$. 100X

in future brazing operations. The tube-to-fin leaks were thought to be caused by excessive use of Nicrobraz alloy, with the resulting dissolution of the tube walls. The bad distortion also tended to aggravate this situation by allowing puddling of the molten brazing alloy. The formation of "hot spots" in the body of the assembly was also thought to be a prevalent condition. A very rapid heating rate was also an important factor in the warpage.

Figure 15 shows the second large unit to be furnace Nicrobrazed. The outward appearance of this heat exchanger is much better than that of the first, and pressure-testing revealed only one leak in the tube-to-fin matrix. However, it is thought that this hole resulted from the use of a faulty tube, since there was no evidence of gross warpage or excessive alloying of the tubes by the brazing alloy. Changes incorporated in the brazing procedure for this second unit were the use of lesser quantities of Nicrobraz, the use of several aspirators to promote more even hydrogen flow between the fins, the build-up of the whole assembly off the can bottom to overcome the drastic initial heating rate, and the use of a slightly lower brazing temperature.

High-Temperature Brazing Alloy Evaluation Program. The results of recent high-temperature oxidation tests and static corrosion tests in sodium hydroxide, sodium, and lithium are shown in Table 14. The high-temperature oxidation tests were conducted in a stream of moist air at 1500°F on specimens of Inconel and type 316 stainless steel brazed with the various alloys. The samples tested in molten sodium hydroxide at 1500°F were A nickel T joints brazed with the various alloys.

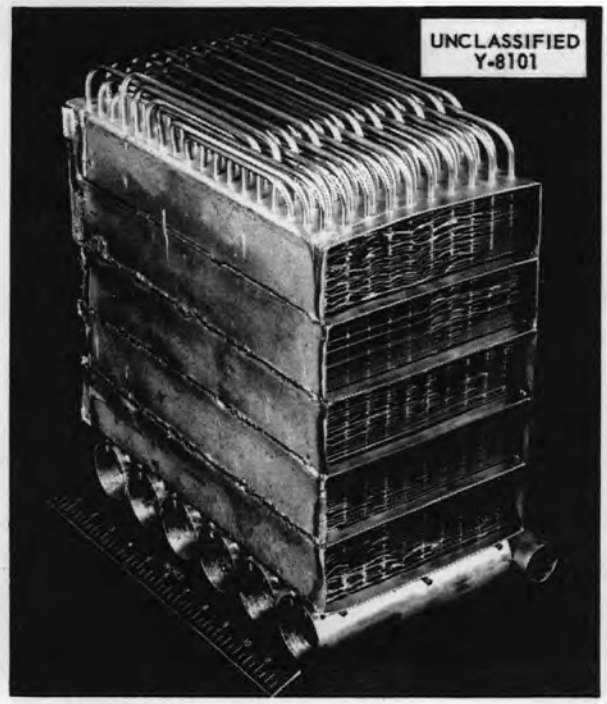

Fig. 14. First Large Heat Exchanger Test Assembly After Nicrobrazing. Excessive fin warpage present.

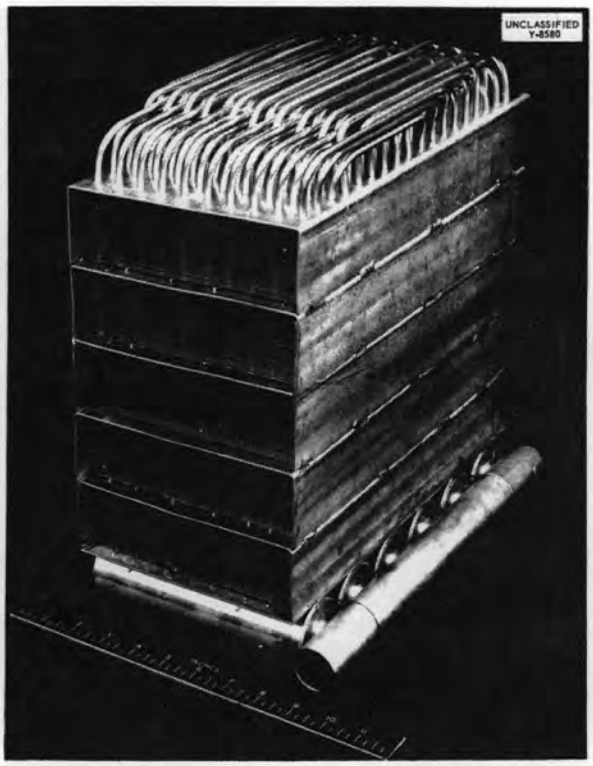

Fig. 15. Second Large Heat Exchanger Test Assembly After Nicrobrazing. Fin warpage negligible.

TABLE 14. RESULTS OF HIGH-TEMPERATURE OXIDATION AND STATIC CORROSION TESTS

BRAZING ALLOY	HIGH-TEMPERATURE OXIDATION		STATIC CORROSION				
	On Brazed Inconel	On Brazed Type 316 Stainless Steel	On Brazed A Nickel In NaOH	On Brazed Inconel		On Brazed Type 316 Stainless Steel	
				In Na	In Li	In Na	In Li
Nicrobraz			Slight	None	Moderate	Slight	Severe
60% Mn–40% Ni			Severe	Moderate	Moderate	Moderate	Severe
60% Pd–40% Ni	None	None	None	Severe	Severe	Moderate	Severe
16.5% Cr–10.0% Si–73.5% Ni	Moderate	None	Fractured during examination	Moderate	Severe	None*	Slight*
16.5% Cr–10.0% Si–2.5% Mn–71.0% Ni	Moderate	None	Fractured during examination	Moderate	Slight	None*	Severe
75% Ag–20% Pd–5% Mn	Severe	Moderate	Severe	Severe	Severe	Severe	Severe
64% Ag–33% Pd–3% Mn	Slight	Severe	Moderate	Severe	Severe	Severe	Severe

*Severe cracking present in joint.

Brazed Inconel and type 316 stainless steel T joints were used as specimens for the corrosion tests in sodium and lithium.

It is interesting to note that the 60% Pd–40% Ni alloy, which exhibited excellent corrosion resistance to all other media tested, was severely attacked by the liquid metals. The extreme attack of sodium on the palladium-nickel brazed Inconel is illustrated in Fig. 16, which shows a sample that was tested for 100 hr at 1500°F. As a check on these results, small specimens of the pure braze metal were immersed in the metal baths. The sample tested in sodium had a weight loss of over 50%, whereas the sample tested in lithium completely dissolved.

Inconel test bars butt-brazed with the 60% Pd–40% Ni alloy were tested at room and elevated temperatures. The average room-temperature tensile strength of these brazed joints was 87,600 psi, whereas those tested at 1500°F had an average tensile strength of 21,000 psi. Check bars of Inconel heat-treated for 5 min at 2300°F were also tested so that the strength of samples subjected to the brazing cycle could be determined. The joint efficiency at room temperature was found to be 100%, whereas at 1500°F, the efficiency was 93%.

Extremely deleterious effects of the high-temperature heat treatment involved in palladium-nickel brazing were not evident in short-time tensile tests on Inconel. Inconel tensile bars, 0.252 in. in diameter, heat-treated for 5 min at the Nicrobrazing temperature of 2100°F, had an average room-temperature strength of 87,300 psi and an average 1500°F strength of 23,200 psi. Test bars heat-treated for 5 min at the palladium-nickel brazing temperature of 2300°F fractured at an average room-temperature strength of 84,500 psi and an average 1500°F strength of 22,600 psi. Thus the larger-grained Inconel has a tensile

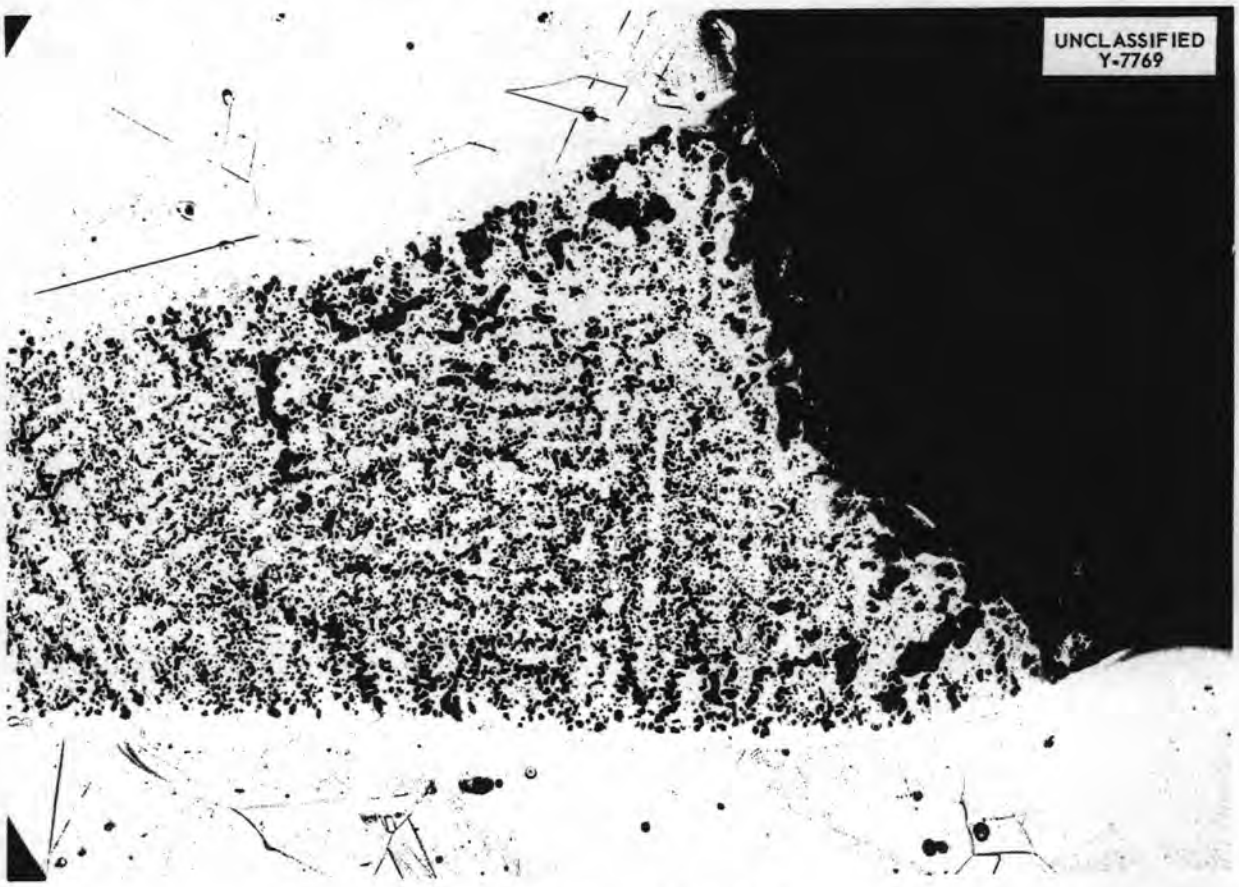

Fig. 16. Inconel Brazed with 60% Pd–40% Ni and Tested in Sodium for 100 hr at 1500°F. Severe attack can be seen. Etched with aqua regia. 150X

strength at room temperature of only 3.2% less than the finer-grained Inconel. At 1500°F, the difference is only 2.6%. All tensile bars in the experiments were machined from the same Inconel rod, and thus there is indication that heat treatment was the influencing factor.

More complete results of the experiments conducted to evaluate the effect of time at the brazing temperature on the joint strength of Nicrobrazed Inconel joints show that this factor is not as important as previous data indicated. The room-temperature strength of these joints is generally much less than the strength of the base Inconel and does not vary appreciably with time at temperature. Only occasionally does a joint exhibit high tensile strength at room temperature, and the previous results were apparently distorted by these infrequent, high values.

A summary of the data is shown in Table 15. Four tensile bars were tested for each brazing time. It is expected that brazing time will have a greater effect with stainless steel because the width of the diffusion zone is generally larger. The composition of Inconel is so similar to Nicrobraz that diffusion is probably somewhat hindered by the lack of large concentration gradients. The tensile strengths of Nicrobrazed Inconel joints at 1500°F have all been consistently high, as previously reported, and the fracture often occurs in the base metal.

An investigation was conducted to determine the effect of joint spacing on the short-time room-temperature tensile strength of Nicrobrazed Inconel joints. Four butt-brazed tensile bars were prepared for each joint spacing of 0.005, 0.010, 0.015, and 0.020 inch. Results were already available on the normally used 0.002-in. joint spacing. The results of these tests are listed in Table 16. The brazing time for each joint was kept approximately the same, that is, 20 minutes.

The results of this investigation indicate that joint spacing is not a critical factor in the room-temperature tensile strength of Nicrobrazed Inconel joints, at least within the ranges investigated. This range should cover nearly all applications, since the effect of a shrink fit would tend to be lost during the furnace-brazing operation and spacings of over 0.020 in. result in extremely poor fitup.

In a further attempt to lower the melting point of the 60% Pd–40% Ni alloy, an alloy was prepared that contained a 10% addition of germanium. This alloy can be consistently brazed at 2150°F, which is in the brazing range of the more common Nicrobraz alloy. Corrosion tests in the molten fluoride fuel salts are being conducted at present, and if this alloy shows resistance to corrosion comparable to the basic palladium-nickel alloy, it may be suitable for some application in which its lower melting temperature is required.

Brazing of Copper to Inconel. The need for a satisfactory brazing alloy for joining copper fins to Inconel tubing and for edge-sealing sheared, Inconel-clad, copper fins has been emphasized. The resultant braze should be resistant to oxidation at 1500°F, should preferably serve as a diffusion barrier against copper penetration into the Inconel during service, and should have a relatively high strength at 1500°F. It is likely

TABLE 15. EFFECT OF TIME AT BRAZING TEMPERATURE ON TENSILE STRENGTH OF NICROBRAZED INCONEL JOINTS

TIME AT 2150°F (min)	AVERAGE ROOM-TEMPERATURE TENSILE STRENGTH OF BRAZED JOINTS (psi)	JOINT EFFICIENCY (%)
5	34,900	40
10	40,100*	46
20	32,900	38
30	31,400	36

*Includes one value of 69,800 psi.

TABLE 16. EFFECT OF JOINT SPACING ON TENSILE STRENGTH OF NICROBRAZED INCONEL JOINTS

JOINT SPACING (in.)	AVERAGE ROOM-TEMPERATURE TENSILE STRENGTH (psi)
0.002	32,900
0.005	35,500
0.010	36,900
0.015	35,000
0.020	39,000

that an alloy other than a copper-base alloy would best fill these requirements.

An experimental, modified, Nicrobraz alloy, which melts at approximately 1850°F, appears very promising, although oxidation tests have not been completed on brazed joints. Several other alloys, with melting points in this same range, have been prepared and high-temperature oxidation tests on these alloys will be conducted. These include alloys of gold and cobalt, gold and nickel, and silver and germanium.

FABRICATION

E. S. Bomar H. Inouye
J. H. Coobs A. Levy[4]

Control Rods. The Fabrication group was asked to conduct a study concerning the adaptation of the iron-cemented boron carbide composition used for the ARE safety rod slugs to the control rods for the GE-ANP reactor. In brief, the specifications for these rods call for a ½-in.-dia by 30-in.-long stainless steel tube filled with a neutron-absorbing material having a minimum boron density of 0.7 g/cm^3. The absorber material should have fair thermal conductivity and should be well bonded to the stainless steel tube. These properties are necessary for dissipation of the heat generated in neutron absorption (7.5 kw per rod, maximum).

Since the iron-boron carbide composition is quite attractive from the standpoint of boron density, several runs were made to determine the maximum length that can be pressed with reasonable uniformity of density. By using a 7-in.-long by ⅜-in.-bore graphite die, several rods that were 73 to 75% of theoretical density and about 3½ in. long were prepared by hot pressing. Attempts to bond these rods to the inside of stainless steel tubes met with little success. The material resisted wetting and consequently was poorly bonded to the tubes.

By using a hydrogen atmosphere, the ability of several materials to wet the hot pressed parts was checked, with the results given in Table 17.

Further attempts to braze the rods with the nickel-boron alloy were unsuccessful. The alloy flowed to the lowest portion of the tube, dissolved additional boron from the carbide, and reacted with the stainless steel tube wall.

A prototype control rod, 30 in. long, has been requested by GE-ANP for reactivity experiments. The heat generated in a reactivity experiment will be small, therefore it will not be necessary to have a brazed couple between the inserts and container. Segments of iron-boron carbide composition have been pressed, the rod will be assembled as soon as end plugs for the tube are fabricated.

ARE Shielding Plugs. A total of seven slugs composed of iron and boron carbide was prepared for shielding plugs in the ARE control system. The slugs were hot pressed and sealed in stainless steel containers by Nicrobrazing.

Tower Shielding Facility Safety Rods. Two safety rods for the Tower Shielding Facility were filled with boron carbide powder. Specification called for a boron carbide apparent density of 1.6 g/cm^3.

A series of checks with various mixtures indicated the maximum tap density to be expected would be about 1.7 g/cm^3 (65% of theoretical). This was obtained using a mixture of 60% (−65 +100 mesh) plus 40% (−325 mesh) B_4C. A starting point for selecting sizes and relative amounts of various boron carbide fractions was supplied by H. T. Kite of Y-12, who has examined a similar packing problem with UO_2 for KAPL.

[4]Pratt and Whitney Aircraft Corp.

TABLE 17. WETTING TEST ON IRON-BORON CARBIDE COMPOSITIONS

ALLOY	TEMPERATURE (°C)	RESULTS
Nicrobraz	1150	Fair wetting of surface, some adherence
BT	900	No wetting
EZ Flow "45"	900	No wetting
Al–12% Si	900	No wetting, oxide film formed
Ni–33% Si	1150	No wetting, oxide film formed
Ni–12% B	1150	Fair wetting, more adherence than with Nicrobraz

The control rod containers were loaded through a $^3/_{16}$-in.-dia hole by using a vibrating funnel. The density of boron carbide in the rods was not as high as expected, it measured only 1.5 g/cm^3 in the first rod and 1.55 g/cm^3 in the second. The reduced packing efficiency may have been caused by classification of the powder during filling or by the additional wall friction of the irregular cavity filled. The rods have been accepted, even though the density falls slightly below that requested.

Solid-Phase Bonding. Two series of samples of solid-phase bonding have been prepared and are awaiting interpretation. Evaluations are to be made of the effect of time on the extent of bonding and of the benefit of electrodeposited chromium in bonding molybdenum to other metals.

Chromium was selected as a trial bonding medium because of its unlimited solubility with molybdenum. Runs have been made with chromium-plated molybdenum vs. nickel, iron, stainless steel, and Inconel at 1150 and 1250°C. One run has been made to check the self-welding of molybdenum at 1500°C.

Special Alloy Fabrication. The development of methods for the fabrication of special alloys was the result of the present need for high-purity Inconel tubing and the subsequent need for other high-temperature alloys. The primary problem to date has been one of lubrication during extruding. None of the extrusions have been entirely successful, failure resulted from either breaking of the mandrel or rupture of the tube.

Molten glass, prepared by a modification of the Sejournet-Ugine process, was selected for the lubricant. This lubricant was chosen because of the lower unit extrusion pressures required with it than with graphite or oil. Another factor in the selection was that with this lubricant the possibility of pickup of carbon and sulfur is reduced. To illustrate a solid rod was extruded successfully by using Necroline, which has a graphite base, but analysis indicated the following changes in carbon and sulphur content:

Carbon content	
As-cast	0.01%
Extruded	0.03%
Sulfur content	
As-cast	0.007%
Extruded	0.017%

For the extrusions made thus far, the extrusion billet was heated in molten lead glass. Unfortunately, a portion of the lead compound in the glass was reduced, and as a result metallic lead precipitated in the batch. The mechanism of this reduction is not, as yet, known. The molten glass was held in a stainless steel container that was seated in and extended above the top of a gas-fired pot furnace. The prescribed extrusion temperature for Inconel is 2300°F, however, with the present heating setup, 2100°F is the maximum temperature obtainable. These factors, no doubt, contributed to or caused the extrusion failures.

One of the ultimate objectives is to obtain tubing that has no inclusions resulting from the addition of malleablizing elements, such as, magnesium, titanium, manganese, and aluminum. To determine which malleablizing elements are necessary, ingots were vacuum cast with no additions, with nominal 0.05% magnesium, and with 0.25% titanium (as Ti-Al-Mn alloy with up to 0.05% magnesium). These ingots have been machined and will be extruded at 2200°F with glass or rock wool as a lubricant.

Columbium Research. Columbium research was initiated because a literature survey revealed the high reactivity of the metal at temperatures above 400°C and because erratic results were obtained in preliminary high-temperature strength tests. Minute quantities of dissolved gases change the mechanical properties considerably, therefore tests of the reactions must be carefully controlled. Of initial interest is the finding of a suitable atmosphere for conducting creep tests. The properties of an argon atmosphere were examined first, and the results listed in Table 18 were obtained. The tank argon used was treated with magnesium perchlorate, titanium sponge at 850°C, and titanium sponge at 200°C.

In addition to argon, a vacuum is being considered as a protective environment for creep tests. The results of 100-hr exposures at 800°C in vacuum are listed in Table 19. Tests for 100 hr at 1000°C are being made.

Oxidation in Air. Tests were made of the stability of columbium oxide at elevated temperatures, with the results shown in Table 20. Since the change in weight for the various samples was extremely small, it was decided to use weight increase as an index for oxidation studies. The tests made above were run in air flowing at 2 liters

TABLE 18. TIME AND TEMPERATURE EFFECTS ON COLUMBIUM IN ARGON

TEMPERATURE (°C)	TIME (hr)	WEIGHT INCREASE (g/cm^2)	HARDNESS INCREASE (VPN)	REMARKS
600	291	0.0005	48	Film of CbO, $A_0 = 4.21$, ductile
800	67	0.0015	106	Black film, not identified
1000	88	0.0026	416	Black film, brittle
1000	89	0.0006	97	Static argon, 5 in. Hg
1000	72	0.0002	85	Capsulated sample in static argon

TABLE 19. EFFECT OF VACUUM ON PROPERTIES OF COLUMBIUM HEATED AT 800°C

PRESSURE (microns)	CHANGE IN WEIGHT (g/cm^2)	CHANGE IN HARDNESS (VPN)	REMARKS
1.0	+0.0046	+271	Brittle, slightly tarnished
0.1	+0.0006	+22	Bright
0.01	−0.0002	−16	Bright

TABLE 20. STABILITY OF ½-g SAMPLES OF Cb_2O_4 IN STATIC AIR FOR 18 HOURS

TEMPERATURE (°C)	WEIGHT CHANGE (g)	REMARKS
1000	+0.0001	Starting material had a few black specks of a lower oxide
1100	+0.0001	Oxide completely white
1200	0	Oxide changed to a yellow color
1250	0	Oxide yellow
1300	−0.006	Oxide yellow
1350	−0.0009	Oxide yellow
1375	−0.0009	Oxide yellow

per minute, the air was dried with anhydrone and passed through a cold trap of acetone–dry ice before entering the furnace.

Oxidation tests were made on columbium by using the conditions outlined and the following results were obtained. In tests at 400°C, there is a short period of slow oxidation followed by a longer period of slower oxidation up to 20 hours.

TABLE 21. COMPARISON OF WEIGHT GAINS AFTER 90-min EXPOSURE OF COLUMBIUM IN FLOWING AIR

TEMPERATURE (°C)	WEIGHT GAIN (g/cm^2)
400	0.00003
600	0.0088
800	0.0465
1000	0.0650
1200	0.0915

Beyond this time, the oxidation rate is linear. The film formed at the end of 30 hr is reasonably adherent. In tests at 600, 800, 1000, and 1200°C, linear rates are observed that become more rapid with increase in temperature. A summary of these results is given in Table 21.

Identification of Oxide Films. X-ray data have been obtained for oxide layers formed in dry air, and thus far all the layers have been identified as Cb_2O_5, of which there are three[5] modifications.

Effect of Moisture on Rate of Oxidation. As a result of the failure of the drying train, a high rate

[5] G. Brauer, *Z anorg u allgem Chem* 248, 1-21 (1941).

of oxidation was observed for a run at 400°C. This aroused interest in the effect of moisture on rates of oxidation at various temperatures. A constant humidity was obtained by passing the air through a saturated solution of NH_4Cl at 25°C. This gives an equivalent moisture content of 18.7 mm of H_2O vapor and was checked to within 0.5% by weighing the moisture absorbed in anhydrone.

The results at 400°C show that the presence of moisture increases the oxidation rate by a factor of 400. At 600°C, a reverse effect was found in that the rate of oxidation decreased to one half that with dry air. The oxidation rate was no longer linear and displayed several breaks that have been duplicated with check runs. At 800, 1000, and 1200°C, the rate of oxidation is not changed by the presence of moisture in the air stream.

ANP Radiators. Radiators in nuclear powered aircraft will be required to handle tremendous quantities of heat. The number of tubes necessary for a bare-tube type of radiator, for this application, would be quite large. Therefore finned-tube radiators are of interest because the number of tubes required would be materially fewer than with the bare-tube design.

A program has been outlined for the evaluation of radiator materials, methods of assembly, and effects of exposure to high temperatures. The materials required for this work have been ordered, and the beginning of active experimental work must await their arrival.

MECHANICAL TESTING

R. B. Oliver J. W. Woods
D. O. Douglas K. W. Reber

Uranium. Specimens of uranium that were beta treated for 80 sec at 730°C and water quenched are being tested at 500°C in vacuum at stresses of 1500 and 2000 psi. When these tests are completed, design curves will be constructed for beta-treated uranium.

One specimen of alpha uranium was stressed to 1850 psi at 500°C alternately in vacuum and purified nitrogen. The test was started in vacuum and this condition was maintained for 1100 hours. Nitrogen that had been purified by bubbling through molten sodium was then introduced in the test chamber at a controlled rate so that the pressure in the chamber was maintained at about 2000 microns. The nitrogen atmosphere was maintained for 175 hr, and the chamber was again evacuated to 0.05 microns pressure, the test was discontinued after an additional 50 hr in vacuum. Table 22 shows the creep rates at various time intervals during the test. When the test piece was examined, it was found that a very tightly adhering gray scale covered the entire test section. X-ray diffraction identified this scale as UN_2, and the thickness was estimated to be about 500 Å units. No evidence of diffusion of the nitrides was revealed by metallographic examination.

TABLE 22. CREEP RATES OF ALPHA URANIUM TESTED IN VACUUM AND NITROGEN

TIME INTERVAL (hr)	ATMOSPHERE	CREEP RATE (%/hr)
100 to 300	Vacuum	0.0016
300 to 600	Vacuum	0.0009
600 to 1075	Vacuum	0.0014
1075 to 1240	Nitrogen	0.0016
1240 to 1290	Vacuum	0.0014

Tests conducted on uranium in gaseous atmospheres were reported previously.[6] Purified dry hydrogen markedly increased the creep rate. Untreated, oil-pumped nitrogen did not noticeably affect the creep rate, but when the chamber was re-evacuated a slower creep rate was observed, which probably showed the effect of oxidation by the oxygen present in the gas. The two tests, one with pure nitrogen the other with commercial tank nitrogen, indicate that nitrogen by itself has little, if any, effect on the creep properties of uranium at 500°C.

Thorium. Tests are now being made to determine the effect of various extrusion rates on the creep properties of thorium. Specimens were machined from rods extruded at 2 and 600 fpm. One half the specimens are being tested in the as-extruded condition and the other one half in the annealed condition. Results of the tests now completed indicate that the slowly extruded specimens show the least initial elongation at any given stress and have the highest ultimate strength. There is some scatter of data of both rapidly and slowly extruded specimens that is related to the position

[6] R. B. Oliver, D. A. Douglas, J. W. Woods, *Met. Div. Quar Prog. Rep. April 20, 1952*, ORNL-1302, p. 67.

in the extruded bar from which the specimen was cut. It is believed that this is a reflection of the varying amounts of mechanical work from the front to the back end of an extrusion. The data for the rapidly extruded specimens, both before and after annealing, are similar, with regard to initial extension at various stresses, to the slowly extruded and annealed specimens. Preliminary orientation studies indicate that there is no significant difference in orientation between rapidly extruded specimens and rapidly extruded and annealed specimens. However, considerable differences exist in orientation of the slowly extruded material before and after annealing.

Inconel. Tests are still in progress to determine the effects of various environments on the creep properties of Inconel. It was shown in previous tests that an air atmosphere increases the time to rupture by a factor of 5 to 10, as compared with tests in an argon atmosphere. Specimens that were oxidized by holding at 815°C for 200 hr are now being tested at 815°C in an argon atmosphere. At the present stage of the test, there is no significant difference in creep properties of these specimens and bright specimens tested in argon at the same stresses and temperature.

Fine-grained Inconel (0.105 mm) specimens have been tested in a purified hydrogen atmosphere at stresses ranging from 2500 to 7000 psi. Table 23 compares the rupture times of tests in hydrogen and in argon at these stresses.

TABLE 23. RUPTURE TIMES OF INCONEL IN HYDROGEN AND IN ARGON

STRESS (psi)	RUPTURE TIME (hr)	
	In Hydrogen	In Argon
2500	429	1750
3500	264	726
5000	144	300
7000	60	96

Inconel specimens that have been given the standard grain-coarsening treatment at 2050°F for 2 hr and as a result have a grain size of 0.250 mm are now being tested in a hydrogen atmosphere. The preliminary results indicate that there is little difference in the rupture times or the creep rates of these specimens in comparison with tests of specimens similarly treated and tested in argon.

Four Inconel test chambers were completed this quarter and tests are being conducted in fluoride No. 27. Table 24 summarizes the results of these tests and compares the rupture life in a fluoride environment with the rupture life in argon and hydrogen.

TABLE 24. RUPTURE LIFE OF INCONEL IN VARIOUS ENVIRONMENTS

STRESS (psi)	RUPTURE TIME (hr)		
	In Hydrogen	In Fluoride	In Argon
7000	60	48	96
6000		125	180
5000	144	142	300
3500	264	420	726

Type 316 Stainless Steel. One test has been completed and one test is in progress on type 316 stainless steel in a hydrogen atmosphere. The data to date do not indicate that there is any significant difference in the rupture times or the ductility of type 316 stainless steel tested in hydrogen compared with specimens tested in argon or in air.

Testing in fluoride No. 14 is continuing. There is some scatter in the data, but the majority of test results show decreased elongation and rupture life when compared with results of tests made in an argon atmosphere.

Tube-burst tests are being made. The tubes are loaded internally with argon under pressure and they are surrounded by a purified argon atmosphere. Preliminary data indicate that there is a marked reduction in rupture life compared with that of flat tensile specimens tested in argon, and in many instances the rupture life is even less than that of the flat tensile specimens tested in a fluoride environment.

PHYSICAL CHEMISTRY

G. P. Smith J. V. Cathcart
W. H. Bridges

Studies of Surface Rearrangements on a Single Crystal of Copper in Contact with a Saturated Solution of Copper in Bismuth. In recent years a large number of papers have appeared in which the role of interfacial free energies and tensions

in determining the microstructure of metals and alloys was discussed.[7] It has been emphasized that a solid metal crystal tends to change its shape in such a way that at equilibrium its surface free energy is minimized. The work outlined below was initiated to study the importance of the variation of interfacial free energy with crystal orientation in determining the surface topography of a metal single-crystal surface.

If it is assumed that the equilibrium form of a single crystal is that geometrical shape which minimizes the total surface free energy of the crystal, then a sphere is obviously the equilibrium shape for the case in which surface energy is independent of crystallographic orientation. In the event that the surface free energy is a function of orientation, the equilibrium shape of a metal single crystal will be a polyhedron whose edges may or may not be rounded. The bounding surfaces would have specific free energies and areas that would minimize the total surface free energy. For large crystals, rearrangement into a polyhedral form would require the movement of very large numbers of atoms over great distances. The driving force represented by the resulting decrease in free energy would be sufficiently small that a very long time would be required for the crystal to attain its true equilibrium form, if such a complete rearrangement would occur at all. This should not, however, prevent the occurrence of local changes in surface topography that would produce configurations of lower surface free energy than the initial surface. It can be shown theoretically that if a macroscopic portion of the surface of a crystal does not coincide in orientation with a bounding surface of the true equilibrium form, there will always exist a hill and valley structure that possesses a lower surface free energy than the initial surface.[8] Further, the hill and valley structure that has a lower surface free energy than any other is that in which the hills and valleys are bounded by surfaces that make up the true equilibrium shape.

One method of testing the variation of surface free energy with orientation is that of maintaining constant all the factors that determine the equilibrium conditions for a crystal except for differences in surface free energy and then observing the changes that occur in the surface topography of the crystal. The experimental technique used in this study was designed to meet these conditions.

The details of the experimental apparatus and procedure were reported previously.[9] They are summarized in the following, and the experimental results are given. A spherical, copper crystal was immersed in a saturated solution of copper in bismuth at 400°C. It suffered considerable surface rearrangement, and as a result many polyhedral prominences formed on the original surface. These prominences consisted of several facet-like faces that are referred to as "pimars" because of their pyramid-like structure. These pimars superficially resembled a hill and valley structure, but closer examination revealed that, in general, the pimars were isolated prominences on a smooth surface. Three crystallographic planes were identified as the bounding surfaces of the pimars. Of these, (111) planes were most important in that they constituted the major bounding faces of the pimars; however, small (110) planes and vicinal planes close to the [311] directions were also detected. The small size of these latter two types of faces together with the high reflectivity of the pimar surfaces made the observation of structural details somewhat difficult. Thus it was impossible to determine whether the pimar faces met at sharp edges or whether these edges were smoothly rounded. The size and density of pimars on the surface of the crystals varied with orientation, both the size and density being greater in the vicinity of [111] and [110] directions than in [100] directions.

One possible explanation of these results can be based on the assumption that the temperature control during experiments was not sufficiently precise. The observed surface rearrangements might then be regarded as a pure growth phenomenon resulting from the alternate solution and deposition of material at the surface of a copper crystal. This explanation was discarded because the temperature fluctuations in the molten nitrate salt bath used as the thermostat for the experiments did not exceed 0.5°C. On the basis of

(7) W. K. Burton, N. Cabrera, and F. C. Frank, *Trans. Roy Soc. (London)* A243, 299-358 (1951), K. K. Ikeuye and C. S. Smith, *Trans. Am Inst. Mining Met. Engrs.* 185, 762-68 (1949), C. G. Dunn, F. W. Daniels, and M. J. Bolton, *J Metals* 188, 1245-48 (1950), K. T. Aust and B. Chalmers, *Proc Roy. Soc. (London)* A204, 359-366 (1950), M. J. Buerger, *Am Mineralogist* 32, 593-606 (1947).

(8) C. Herring, *Phys. Rev.* 82, 87-93 (1951).

(9) G. P. Smith, Jr., J. V. Cathcart, and W. H. Bridges, *Met. Div. Quar. Prog. Rep. Apr. 30, 1952*, ORNL-1302, p. 59.

previous supersaturation tests, it is believed that these variations were not sufficient to produce the observed changes.

It appears more reasonable to assume that variations of surface free energy with orientation were responsible for the surface rearrangements. The following hypothesis is based on this assumption, it is only tentative and is proposed as a working hypothesis for future experiments.

As explained above, it can be predicted on theoretical grounds that a large single crystal in an equilibrium state except for free energy differences between crystallographic planes could reach a lower free energy state by undergoing a surface rearrangement that would result in the formation of a unique hill and valley structure on the surface of the crystal. These theoretical predictions were closely approximated by the experimental results. It is believed that the formation of facets on the original surface resulted in a decrease in the total surface free energy of the crystal. The prominence of the (111) planes on the pimars was interpreted as indicating that for a copper crystal in contact with a saturated solution of bismuth, the (111) crystallographic planes possess the lowest surface free energy of any plane. The occurrence of (110) planes suggests that these planes are also stable at equilibrium, although their small extent relative to the (111) planes and the failure to observe pyramids consisting entirely of (110) planes near the [100] directions indicates that the (110) planes do not have a sufficiently low free energy to be in equilibrium.

It would seem unlikely that a vicinal plane (such as that observed near the [311] directions) would be a stable part of an equilibrium form. The occurrence of vicinal planes as parts of the bounding planes of the pimars was probably a result of the growth process. The fact that the pimars occurred as more or less isolated prominences on a smooth surface suggested that the mechanism of their formation involved point nucleation. The terms "nucleation" and "growth" are used here to distinguish the proposed mechanism from one in which the entire surface of the crystal is transformed continuously into a hill and valley structure. For these reasons, it is considered that pimars are nucleated at a point and grow both laterally and vertically. Nucleation could be aided by lattice distortions, clustering of impurity atoms, and statistical clustering of self-adsorbed atoms or by some other similar process.

The process of the nucleation of a pimar on a crystal surface may be regarded as the two-dimensional analog of three-dimensional bulk nucleation. In this latter case, nuclei of an alpha phase forming in a beta phase at the transition point remain unstable until they reach a certain critical size, because their formation requires the production of new interfaces. The total surface free energy of such an interface is greater than the total volume free energy of either the alpha or the beta phase, and until the nuclei grow to such a size that the extra energy of their surfaces is compensated for by the lower volume free energy of the new phase, they remain in an unstable state.

Similarly, the free energy of a pimar may be regarded as the sum of two terms that express the surface and edge free energies, respectively, of the pimar

$$\gamma_f = \gamma_s(r^2) + \gamma_e(r) , \qquad (1)$$

where γ_f is the specific surface free energy of the pimar, γ_s represents the specific surface free energy of the bounding planes of the pimar and is a function that depends on the second power of the radius of the pimar, and γ_e is the specific edge free energy that depends only on the first power of the radius. When the pimar is very small, that is, when it is still in the nucleus state, the value of γ_f will be determined largely by γ_e. As growth proceeds, γ_s increases at a faster rate than γ_e until, at a certain size, the two terms become equal. Beyond this point, γ_s is predominant in determining the value of γ_f.

The change in free energy during the formation of a pimar may be expressed most conveniently in terms of the change in free energy per unit area of original surface. If $\Delta\Gamma_T$, Γ_f, and Γ_o represent the total change in surface free energy, the total surface free energy of a pimar, and the total surface free energy of the original surface which is covered by the pimar, respectively, and if a_f and a_o are the areas of the pimar-covered and original surfaces, respectively, the change in free energy per unit original area is given by

$$\frac{\Delta\Gamma_T}{a_o} \equiv \overline{\gamma}_T = \frac{a_f}{a_o}\gamma_f - \gamma_o , \qquad (2)$$

where γ_f and γ_o are the specific surface free energies of the pimar and original surface, respectively. By using equation (1),

$$\bar{\gamma}_T = \frac{a_f}{a_o} \gamma_s(r^2) + \gamma_e(r) - \gamma_o . \quad (3)$$

Since pimar formation occurs isothermally and spontaneously, a net decrease in surface free energy is to be expected for the production of a stable pimar. When the pimar is very small, however, the first term on the right hand side of Eq. 3 is governed by γ_e, the unit edge free energy, and since γ_e for a very small pimar is greater than either γ_s or γ_o, $\bar{\gamma}_T$ will at first be a positive quantity and then become negative when the pimar size increases to the point where γ_s determines the value of the first term in Eq. 3. γ_s must, of course, be less than γ_o, since it was assumed initially that the surface free energy of the pimars was less than that of the original surface. Thus the formation of a pimar may be regarded as a nucleation and growth phenomenon that requires a certain nucleation energy to initiate growth.

The influence of small surface strains in initiating pimar formation is of interest in connection with the question of nucleation. It was found that the density of pimars formed on a crystal was in direct relation to the amount of strain in the crystal. The density of pimars was least on crystals that had been grown in the desired experimental shape and whose only subsequent surface treatment had consisted of a deep electropolish. Crystals that were grown in the shape of cylindrical rods and turned into shape on a lathe showed an increase in pimar density, despite the fact that they had previously been carefully mechanically and electrolytically polished and had been annealed at 400°C for 24 hours. In these crystals the pimars tended to be aligned along intersections of slip planes with the surface of the crystal. The most pronounced effect of strain was exhibited by a crystal that had been intentionally stressed (about 4%). In this case, the facet density was very high. Although it is not possible to draw any quantitative conclusions from these facts, they indicate the possibility that small surface strains may be the source of the energy required in the nucleation process described above.

It should be pointed out that once a pimar nucleus has reached such a size that it is no longer unstable, no further energy is required for its continued growth. Even if no screw dislocations terminate on its surface, the pimar, by the nature of its geometry, possesses several reentrant edges at its base from which growth of successive new atomic layers can originate.

One interesting result of this hypothesis is that it provides an explanation for the observed variation in pimar density with crystal orientation. Thus relatively few pimars were detected near [100] directions as compared with those detected near [111] and [110] directions. A pimar formed close to a [100] direction was observed to be an eight-sided pyramid consisting of four (111) planes and four (110) planes. Both these planes make large angles with a (100) plane, so the decrease in surface free energy occasioned by the appearance of (111) and (110) planes was in some measure counterbalanced by the relatively large increase in surface area required for the formation of the pimar. If it is assumed that the surface free energy of a (100) plane does not differ by too large a factor from that of the stable (111) and (110) surfaces, it follows that the nucleation energy for a pimar near a [100] direction should be higher than that for a pimar near [111] and [110] directions. Hence, the nucleation frequency in the (100) region should be higher than in the latter two regions.

Future Work. It is planned to perform a series of experiments designed to study the early stages of pimar formation. This study should provide a ready means of testing the hypothesis outlined above. Further examination of well-developed pimars will also be carried out to make sure that no bounding planes of very small areas have been overlooked.

CERAMICS RESEARCH

J. M. Warde
C. E. Curtis
L. M. Doney
S. D. Fulkerson
J. A. Griffin
J. R. Johnson
A. J. Taylor
G. D. White
T. N. McVay, Consultant
T. S. Shelvin, Consultant

CERAMIC COATINGS FOR METALS

Radiator Coatings (ANP). A project for the application of a ceramic coating to nickel radiator parts awaits the delivery of the radiator assembly.

Fluoride-Resistant Coatings. Work started on the development of a fluoride-resistant coating for application to mild steel for the construction of the tanks to be used in the early stages of the diffusion studies has been held in abeyance during the last quarter because of the lack of personnel.

High-Boron Coatings. Work was carried out on the development and method of application of a ceramic coating containing a minimum of 10% boron to metal surfaces for use in reactor shielding. A lead-borate enamel was developed that could be successfully flame-sprayed in a 20-mil coating on 20-Ga. steel. The batch composition of this enamel is:

B_2O_3	35.0%
PbO	62.5%
ZnO	2.5%

An investigation of flame-spraying techniques indicates that coatings up to 15 mils thick can be successfully applied to mild steel plate that is up to $\frac{1}{16}$ in. in thickness. To successfully apply this coating to a 5-ft square mild steel plate $\frac{7}{8}$ in. thick, to be used in the shielding test, it was found necessary to dry coat the piece and fire the coating to maturity in a furnace at 1350°F.

RADIATION DAMAGE STUDIES

Further work in the radiation damage studies awaits the results of exposures of ceramic specimens at Hanford. Some additional studies of the banding observed in specimens of quartz irradiated with a cobalt source were made (Fig. 17). It is believed that these bands are *f*-center phenomena resulting from trace impurities in the quartz. It is possible that some correlation of geologic history with the size and nature of the bands may be found.

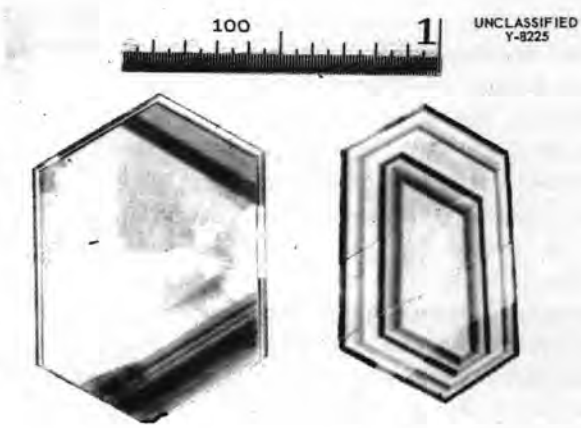

Fig. 17. Quartz Specimens After Irradiation with a Cobalt Source. Specimen on right from Brazil; specimen on left from Arkansas.

DEVELOPMENT OF CERMETS FOR REACTOR COMPONENTS

The Cr-Al_2O_3 cermet fabrication studies have resulted in the successful preparation of disks 1 in. in diameter and 20 mils thick. Several sandwich disks were also made that contained a thin layer of UO_2 mixed with 70% Cr–30% Al_2O_3. Annular rings have been formed of the 70% Cr–30% Al_2O_3 composition containing about 8% UO_2 in sandwich form. In-reactor tests of these cermets are now being contemplated. A ZrC-Fe cermet was fabricated as a possible material for pump parts, seals, and bearing materials. This cermet, along with Kennametal 151-a, has been tested for corrosion resistance in fluorides, sodium, and lead. These materials appear to be very promising. The Kennametal 151-a showed no attack at 800°C for 100 hr in sodium, lead, and fluoride No. 14. A slight surface leaching was observed on the ZrC-Fe cermet in both sodium and fluoride No. 14.

The development of fuel elements using combinations of SiC-Si and USi_x was started. The SiC-Si body is prepared by heating at 1000°C for 1 hr a

mixture of 50% graphite (2 micron) and 50% wheat flour. The resulting porous body is then placed in a graphite container together with powdered silicon, and the container is heated by resistance to 2000°C, at which temperature silicon carbide is formed, with an accompanying exothermic reaction, while molten silicon is simultaneously absorbed by the body. The resulting cermet appears to have a well-bonded structure that is free from voids. Further work is in progress to determine the physical properties of this material.

An investigation of the preparation of USi_x has commenced. A material containing about 90% USi_2, 5% USi_3, and 5% UO_2 has been successfully prepared by heating uranium metal in contact with silicon at 1700°C. It is necessary to have a very pure argon or helium atmosphere for this reaction.

Preliminary designs of an in-reactor high-temperature test rig were made. It is proposed that a design be prepared for a small chamber about 4 in. in outside diameter and 12 in. long with two concentric compartments, the inner compartment will be for containing ceramic fuels, and the outer compartment will contain water cooling coils that will serve to cool both the container and any hot gases from the inner fuel element chamber. The following gas cycle is to be used· out-of-reactor pump to inner chamber to outer chamber to out-of-reactor radioactive counting rig to out-of-reactor pump. The out-of-reactor pump is to be used to provide flow rates over the fuel element of the order of 200 fps.

OXIDE CERAMICS

Thorium Oxide. In determining the properties of thorium oxide for possible application as a reactor material, it was shown that firing temperatures of 1400 and 1600°C (held for 1 hr) are insufficient to vitrify pure thorium oxide. Firing at 1800°C and the effects of additions of alumina, silica, zirconia, and of other ingredients in promoting vitrification at lower temperatures are being investigated. Measurements of the resistance of thoria to autoclaving are being conducted through R. B. Briggs' HRE Group, with the use of fused thoria pellets obtained by this laboratory from the Norton Company.

Three thoria cylinders (solid) 2 in. high and 1 in. in diameter were slip-cast and fired at 1600°C for the Experimental Engineering Department. The cylinders are to be used in testing the thermal conductivity of thorium oxide at room temperature.

Uranium Oxide. Hot-pressed specimens of uranium oxide have been transmitted to R. B. Briggs, HRE Group, for autoclave testing.

FABRICATION OF SPHERES FROM CERAMIC MATERIALS

A laboratory method for producing small ($\frac{1}{8}$ to $\frac{1}{2}$ in. in diameter) spheres from powdered ceramic materials is being worked out. This technique will be employed for the production of uranium oxide pellets and will be useful for various other applications.

VAPOR COATING OF BERYLLIUM OXIDE

The coating of graphite by the vapor decomposition method has been described by Kertesz *et al.*[1] Because hot-pressed beryllium oxide samples have, in the past, shown a tendency toward particle disintegration when dynamically tested in liquid NaK, it was thought that a coating of silicon, silicon carbide, or some of the refractory metals might retard, if not completely stop, this disintegration. Accordingly, an apparatus for vapor deposition experiments has been rigged and an investigation commenced under the joint auspices of the Ceramic Laboratory and the ANP Chemistry Section. So far, it has been established that hot-pressed beryllium oxide specimens can be coated by this method by passing $SiCl_4$ vapor in a hydrogen atmosphere over heated specimens of beryllium oxide. It was found that unless the specimen temperature is kept in the range 900 to 950°C, and the flow of vapors is kept at a very low rate, the coating is deposited too rapidly and it is too thick and too uneven. Such a coating spalls off readily when cooling. For silicon carbide coatings, in the preparation of which $SiCl_4$ and hydrogen vapors are first bubbled through liquid toluene and then passed over the heated sample, the same operating conditions hold. This popping off of the heavy coating is due, in part, to the wide difference in the coefficients of expansion of the materials involved. A specimen of silicon that was successfully coated with a thin and uniform coating was submitted to the ANP Experimental Engineering Section for a 200-hr dynamic test in liquid NaK. Results of this test are not yet available. Also, a specimen of beryllia presumably

[1] F. Kertesz, H. C. Brassfield, and L. M. Doney, *Coating Graphite with Silicon and with Silicon Carbide by the Vapor Decomposition Method*, NEPA-1553 (Aug. 1, 1950).

coated with silicon carbide has been submitted for x-ray determination. It is planned to try coatings of zirconium, molybdenum, titanium, deposited in a similar manner, by using a volatile compound of these metals as a source.

INSULATING END-CAP DEVELOPMENT

Work has commenced on developing insulated end caps for Hanford-type slugs. It is proposed to fasten disks of ceramic materials inside of the aluminum end caps during the slug canning operation. The purpose of the caps will be to equalize the heat flow from the center of the slug to the surface. A number of disks of various ceramic materials, such as SiO_2 glass, forsterite, zircon, and alumina porcelain, have been prepared. These disks are 30 mils thick and 1.1 in. in diameter. It was originally intended to make up canned slugs with the ceramic disks in place and forward them to Hanford for tests. Unfortunately, the Y-12 canning line has been shut down and the expense of setting up to get the job done here is prohibitive. The disks have therefore been sent to Hanford for make-up of the slugs.

UNIFORMITY OF BERYLLIUM OXIDE BLOCKS

A study of the physical structure of the beryllium oxide blocks to be used in the ARE was made to aid in the interpretation of BeO-NaK compatibility test data. These blocks, fabricated by the Norton Company, were made by hot-pressing beryllium oxide powder. They are hexagonal blocks $2\frac{1}{8}$ in. on a side, $3\frac{11}{16}$ in. in diameter across the center of the faces, and 6 in. long. They are fabricated with a center hole running axially through the block, the diameter of the hole (depending on the position of the block in the reactor core) is $\frac{1}{2}$, $1\frac{1}{8}$, or $1\frac{3}{4}$ inches. A visual examination was made of about 30 blocks of the type having a $\frac{1}{2}$-in.-dia hole. These blocks had been sawed in two on a plane perpendicular to the long axis. It was observed that in all cases the core of the blocks had a different physical structure than that of the outer portion of the same blocks. In order to study the core structure, six blocks that had not been sawed were soaked in fuchsin dye for 12 hours. The dye is absorbed most in the more porous areas in the block, Fig. 18 shows the typical soft-core structure noted in all the dyed specimens. Samples taken from the inside and outside surfaces of these blocks showed density variations from 2.80 to 2.83 at the outside, which decreased to 2.26 to 2.43 at the inside. The apparent porosity of the dense portion of the block is practically zero, compared with values up to 23.3% for the soft core. Table 25 gives results of density, apparent porosity, and water absorption measurements for specimens cut from various portions of the block.

Blocks that have a $1\frac{1}{8}$-in.-dia central hole are being split longitudinally so that the two halves can be placed around a cooling pipe. With the blocks split, a large amount of inner surface will

TABLE 25. DENSITY, POROSITY, AND WATER ABSORPTION MEASUREMENTS OF VARIOUS SECTIONS OF THE BERYLLIUM OXIDE BLOCK

SOURCE	WET WEIGHT, W (g)	DRY WEIGHT, D (g)	$W-D$	ABSORPTION, $\frac{W-D}{D}$ (%)	SUSPENDED WEIGHT, S_Δ* (g)	$W-S_{\Delta\Delta}$**	DENSITY (g/cm^3)	POROSITY $\frac{W-D}{W-S}$ (%)
Outer edge	1.3612	1.3609		0	0.881	0.4802	2.83	0
	1.8459	1.8458		0	1.187	0.6589	2.80	0
	2.0859	2.0860		0	1.350	0.7359	2.83	0
Core	1.3957	1.2789	0.1168	9.13	0.846	0.5497	2.33	21.25
	1.3555	1.2661	0.0894	7.06	0.835	0.5205	2.43	17.18
	1.1778	1.0680	0.1098	10.28	0.707	0.4708	2.27	23.32

*S_Δ = weight suspended in water.
**$S_{\Delta\Delta}$ = equivalent to volume.

Fig. 18. Dye-treated Beryllium Oxide Block Showing Porous Central Section.

be exposed to the coolant material. This inner surface is low-density material that is particularly susceptible to NaK corrosion. To determine the extent of the low-density region, a random sample of these blocks was soaked in fuchsin dye for 12 hr and specimens were cut from selected localities in the block. Figure 19 shows the density and per cent porosity placed on the block in the location from which the sample was taken. The dark shaded areas on the right of the block indicate the porous portions shown up by the penetration of the dye. Five samples of blocks with a $1\frac{3}{4}$-in.-dia central hole were soaked in dye and were also found to have a porous central core.

A general observation was made regarding the prevalence of cracks in all the blocks examined. All the blocks have at least one crack, and some blocks contain several cracks. In some cases these cracks are visible at the surface of the block, but in the majority of the blocks the cracks are confined to the interior portion. These cracks are quite narrow and contribute only slightly to the porosity. The presence of one of these cracks may be observed in Fig. 19.

The porous condition developed in the hot-pressed beryllium oxide blocks is a defect caused by fabrication. A probable cause of the defect is that the hot-pressed die had too tight a fit on the top and bottom punches around the central pin, which would cause binding and therefore uneven pressure application. A further factor is faulty filling of the die, which would cause bridging of the powder around the pin. Other factors, such as too short time of application of pressure, too short time of holding at pressing temperature, uneven temperature distribution in the beryllium oxide powder because ot too rapid heating, cooling of the die to room temperature without extracting the core pin, etc., could also have affected the final density.

PETROGRAPHIC EXAMINATION OF FLUORIDES

A considerable amount of work has been done in connection with the ANP liquid fuel program. This has included a study of reduction products found in loops, the identification of compounds found in the various fluoride systems and compositions, and the determination of the optical properties of carefully prepared fluoride compounds.

The optical properties of the red $2ZrF_4 \cdot UF_3$ and the olive-drab $UF_3 \cdot UF_4 \cdot 4ZrF_4$ compounds have been determined. These appear to be relatively pure, but x-ray-diffraction patterns have not as yet been obtained. The compounds are similar to those found in loops to which NaK was added. However, a different olive-drab compound was found in a stainless steel capsule containing ZrF_4 and UF_4 heated at an elevated temperature. Evidently the metal of the capsule reduced the UF_4.

The optical properties of Na_2UF_6, K_3UF_7, Na_3ZrF_7, Li_2ZrF_6, and Cs_2ZrF_6 have been determined, and some progress has been made in the identification of other compounds in the LiF-ZrF_4 and CsF-ZrF_4 binaries, as well as in the UF_3-UF_4-ZrF_4 ternary system.

It is proposed to assemble all the optical data that have been collected for the various new fluoride compounds, and, after careful scrutiny, this material will be submitted for publication.

Progress has been made in the identification of a low index of refraction phase that is usually present in considerable amounts in both fluoride No. 27 and fluoride No. 30. The identification of this compound has been difficult because to date it has not been possible to prepare the pure compound. However, new evidence indicates that it has a slightly higher ZrF_4 content than $NaZrF_5$ has.

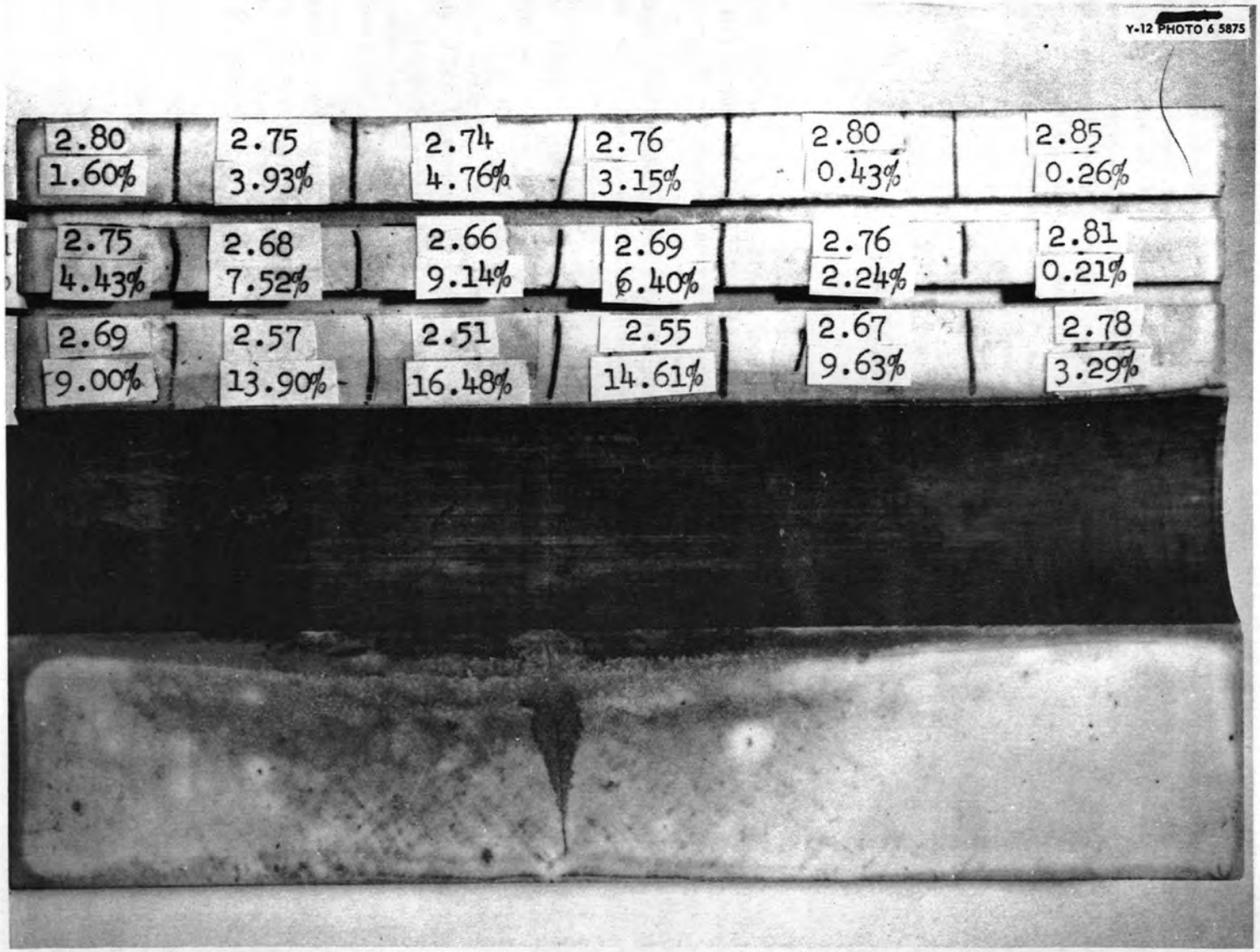

Fig. 19. Density and Per Cent Porosity at Various Locations in a Full-Size, ARE, Beryllium Oxide Block.

Lignite. A large number of particle size determinations have been made on air-separated fractions of both air-dry lignite and lignite ash. The principal impurities found in the lignite studied were quartz, clay, gypsum, and jarosite. These minerals are for the most part concentrated in the coarser particle-size fractions. Also, at least three new minerals were formed when the lignite was ashed at 1000°F. This mineral formation may have an important bearing on the subsequent treatment of the ash.

Examination of Chlorides. In connection with the ANP fuel program, optical data have been determined on compounds in the UCl_4-NaCl and UCl_4-KCl systems. Two compounds have been found in the UCl_4-NaCl system: a pale green compound, $2NaCl \cdot UCl_4$, and a yellow-green uranium-rich compound for which the composition is not known. Since it has been impossible to obtain a homogeneous sample, the latter compound probably melts incongruently on the high-uranium side of the system. In the UCl_4-KCl system, three compounds have been found: $2KCl \cdot UCl_4$, a pale green phase, $KCl \cdot UCl_4$, a pleochroic phase that is blue-green in color, and a yellow-green phase for which the composition is not certain.

REACTOR COMPONENT FABRICATION

J. E. Cunningham

THORIUM-URANIUM FUEL ELEMENT

R. J. Beaver J. W. Geer

Fabrication studies were initiated on a converter-breeder type of thorium-uranium alloy fuel plate for possible service in a H_2O-cooled and -moderated "package" reactor. There is interest in such a fuel element because the long service life obtainable would result in substantial savings in both fabrication and chemical processing costs, as well as in fuel investment.

Although when in use there will be an ultimate need for either zirconium or stainless steel cladding, the initial work was done with aluminum cladding, primarily to expedite radiation damage testing of the alloy in the MTR. The main reasons for the choice of aluminum are (1) it avoids the use of dissimilar metals in intimate contact in the same system or the possibility of galvanic corrosion, and (2) it can readily be stripped chemically from the alloy to facilitate dimensional and physical property measurements after irradiation.

Several melts of thorium-rich alloys, 1 to 5 wt % uranium range, were successfully prepared in the arc-melting furnace. Chemical analysis verified the intended composition, within the accuracy of the determination.

The alloy can be readily hot or cold worked. Room temperature hardness values of the alloy are given in Table 26.

The alloy can be metallurgically bonded to commercial 2S-grade aluminum by hot rolling in the 400 to 450°C temperature range with a total reduction in thickness of 8 to 1. Jacketed billets rolled at temperatures in excess of 450°C show the presence of the brittle $ThAl_3$ compound at the alloy-aluminum interface. It is not necessary to evacuate jacketed billets that are rolled below 450°C.

Like unalloyed thorium, the uranium-thorium alloy tends to "ball-up" on the leading and trailing ends when rolled in a composite pack with aluminum cladding. The resulting nonuniformity in

TABLE 26. ROOM-TEMPERATURE HARDNESS OF THORIUM-RICH ALLOYS

ALLOY COMPOSITION	CONDITION	HARDNESS IN DPH (10-kg load)
Unalloyed Ames thorium metal	Cold worked 30%	99
1.1% U–Th	Cold worked 33%	116
1.1% U–Th	Cold worked 33% and annealed 6 hr at 800°C	89
1.1% U–2% Zr–Th	Cold worked 33% and annealed 6 hr at 800°C	69

core thickness is believed to be due to the difference in plasticity between the two materials at rolling temperatures.

This defect can be partly corrected by using either 24ST- or 52S-grade aluminum to back up or stiffen the 2S-grade aluminum cladding. However, this results in either a 5- or 7-ply sandwich, depending on whether or not 2S-grade aluminum is desired as the outer cladding material.

Three Alclad, enriched, uranium-thorium alloy plates, 8 in. long, 1 in. wide, and 0.072 in. thick, and one plate 28 in. long, 1 in. wide, and 0.072 in. thick, were fabricated for irradiation testing in the MTR. The alloy core used in the preparation of these plates was composed of 98.8% thorium and 1.2% highly enriched uranium metal.

The cladding techniques developed and proved to be successful for cladding Ames thorium metal with zirconium were tried on a 4% uranium-thorium alloy. The brazing and the diffusion-anneal cladding techniques appear to work equally well on this thorium-rich alloy.

The brazing-in-vacuum technique, in which a brazing alloy of 22% zirconium-thorium alloy is used, was fully described in a previous report.[1] The diffusion-anneal method consists of picture framing the alloy in zirconium and canning the entire compact in a stainless steel jacket for oxidation protection during hot rolling. After evacuation through an exhaust tube, the assembly is sealed by hot forging. The use of NBS ceramic frit A-418 coated on the stainless steel prevents the formation of the iron-zirconium eutectic during the diffusion-anneal treatment.

FABRICATION OF URANIUM-ALUMINUM ALLOY COMPONENTS

J. H. Erwin
J. N. Hix
G. E. Cooley
G. D. Goldston
H. J. Wallace
W. W. Proaps
E. R. Turnbill

MTR Experimental Studies. Work on the problem of improving the operational performance of the MTR continues. Techniques have been found that minimize the amount of poisonous brazing flux entrapped in the fuel element during manufacture. The V_{Al}-to-V_{H_2O} ratio can be safely lowered by cautious modifications of the fuel element design. The proposed substitution of an aluminum extrusion for the lower stainless steel bearing section in the shim control rod will not adversely affect either operational control or the mechanical stability of the rod.

Results of this work were discussed in detail with members of the Phillips Petroleum Co. and the Idaho Operations Office at a meeting held in December.[2] Recommendations were (1) that one control rod of the new design be constructed and tested at ORNL, (2) that an experimental loading of 23, thin, side-plate units be fabricated according to the latest techniques to be ready for the next reloading on about February 1, 1953, and (3) that the Phillips Petroleum Co. investigate a fuel assembly design that features more fuel concentrated in the upper half of the element than in the lower half.

Studies to Eliminate Flux Entrapment. Although not known with certainty, it was strongly suspected that the fuel element was being poisoned by simple mechanical entrapment of brazing flux, and experimental work on the problem of removal followed this lead. Another possible mechanism was that of lithium alloying with the aluminum-silicon braze metal in much the same manner that sodium is used to modify this particular alloy.

Experimental work was conducted in two steps. The initial phase consisted of investigating the effect of higher brazing temperature, joint design, and techniques of applying the flux. No attempt was made to alter the composition of the flux. This work is now complete and the important results are summarized in Table 27.

All tests were run on full-sized, dummy, aluminum fuel units. After brazing, the units were carefully dissolved by the Chemical Technology Division and the solution was analyzed for lithium content by the flame photometer method. The accuracy of the determination is better than 2 ppm at a 95% confidence level. In all but the first test, brazing flux from the same batch was used to remove the variable of change in flux composition. Analysis showed that this flux contained 4.72% lithium and 54.0% chlorine.

The amount of chlorine and flux contained in each unit (shown in Table 27) was calculated on the basis of the above analysis. The use of mercuric nitrate as a catalyst in the dissolving

(1) J. E. Cunningham *et al.*, *Met. Div. Quar Prog Rep. July 31, 1952*, ORNL-1366, p. 14.

(2) J. E. Cunningham, *MTR Fuel and Control Rod Element Meeting*, ORNL CF-53-1-150 (Jan. 14, 1953).

TABLE 27. RESULTS OF BRAZING TESTS TO ELIMINATE FLUX ENTRAPMENT

TEST ASSEMBLY	BRAZING CYCLE		AMOUNT PER UNIT (g)			CALCULATED LOSS IN $\Delta k/k$ IN ACTIVE LATTICE DUE TO		
	Temperature (°F)	Time (min)	Li	Cl	Flux	Li	Cl	Li + Cl
X-1	1100	37	1.26	14.41	26.69	2.52	2.67	5.19
X-13	1105	35	0.57	6.52	12.08	1.13	1.22	2.35
X-21*	1105	33	0.17	1.94	3.60	0.35	0.37	0.72
X-22*	1115	31	0.09	1.04	1.93	0.19	0.20	0.39
X-23**	1115	31	0.06	0.76	1.40	0.13	0.14	0.27

*Side plate, $\frac{1}{8}$ in. thick, with shallow groove joint.

**Same as X-21 except for change in technique of applying flux.

step prevented a direct check on the chlorine content in the dissolved assembly solution.

The values of loss in $\Delta k/k$ were calculated on the basis of a 3- by 9-slab loading arrangement of 140-g elements with a total poison cross section of 7700 cm^2.

The results of the brazing tests show that the combination of higher brazing temperature, more shallow groove joint, and flooding of the side plate with an excess of flux reduced the amount of lithium, and presumably chlorine, by a factor of 21. Attempts to braze at 1120°F were not successful because the braze metal alloyed excessively with the 2S-grade aluminum side plate at this temperature.

In the second phase of the investigation, the work was centered on the problem of developing a new brazing flux that is essentially free of lithium and chlorine. Several special fluxes prepared by Alcoa and Permalatem were tested, with unsuccessful results.

A new bromide-base flux, developed at ORNL, showed promise during initial testing. The flux is prepared from a base mixture of 20 parts of barium bromide, 60 of calcium bromide, and 20 of sodium bromide, with 2 parts of either $CaCl_2$ of $SrCl_2$ and $1\frac{1}{2}$ parts of $ZnCl_2$ added. Testing is incomplete.

Design and Fabrication Studies to Improve the Al-to-H_2O Ratio. Another approach to enhance the performance of the reactor is to alter the fuel element design to obtain a lower V_{Al}-to-V_{H_2O} ratio in the active core. Structurally, the present fuel element is over-designed for service in the MTR. Study revealed, however, that any contemplated design change is limited largely by the hydraulics of the present system, hence, only minor changes in the fuel element were considered. The modifications considered were guided, generally, by the following factors (1) an Al-to-H_2O ratio in the active core of less than 0.60 would be desirable, (2) the external dimensions of the fuel unit would remain the same, (3) any fuel component member altered would not be substantially weakened structurally, (4) effects on water velocity and flow area would be investigated, (5) no similar change would be made in the fuel section of the shim control rod; (6) manufacturing cost would not increase.

The Al-to-H_2O ratio of a single fuel element of the existing design ($\frac{3}{16}$-in.-thick side plate and 0.060-in.-thick fuel plates) is 0.716. This ratio increases slightly to 0.731 for the entire 3- by 9-slab loading arrangement because of the additional aluminum in the four shim control rods.

The first change investigated was that of reducing the side-plate thickness from $\frac{3}{16}$ to $\frac{1}{8}$ inch. This lowered the Al-to-H_2O ratio in the active lattice to 0.689 and increased k_{eff} by approximately 1%. The water flow area increased 2.5%

A dozen or more full-sized units of this design were successfully mocked up according to specifications, and no manufacturing difficulties were found. Subsequently, an enriched fuel element of the same design was fabricated and transferred for service in the LITR.

The second modification considered was that of decreasing the cladding on the fuel plate from 20

to 15 mils. The combination of this change plus the thin-side plate drops the Al-to-H_2O ratio in the active lattice to 0.569, but the water gap increases from 117 to 128 mils.

No attempt was made to fabricate this particular unit because of the objectionable increase in water-gap thickness. Instead, another fuel plate was added to the unit to bring the water-gap thickness back to 118 mils.

A 3- by 9-slab loading of these 19-plate elements has an Al-to-H_2O ratio of 0.600, and, more importantly, it increases k_{eff} by approximately 4%. A portion of this gain, however, is due to the extra fuel present because of the added plate. The water-flow area is increased appreciably, that is, by 8.2%.

It should be pointed out that this change does not materially weaken the fuel plate structurally, because the strength of the member is determined largely by the core alloy, which has been altered. The yield strength of annealed 2S-grade aluminum, for instance, is 5000 psi, whereas the 17% uranium-aluminum alloy has a yield strength of 9000 psi, based on a 0.2% offset at room temperature.

The change does proportionately lower the amount of corrosion protection afforded. It is felt, however, that 15 mils of cladding would be more than adequate to protect the alloy core, which, by itself, exhibits fair corrosion resistance to water. Examination of elements at ORNL after ten months of service in the Bulk Shielding Reactor failed to reveal any pitting type of attack or other corrosion phenomena. Service in static water, such as in the BSR, is more severe corrosion-wise than is the 30-fps water velocity condition that exists in the MTR.

Neutron-wise, it is certainly advantageous to replace aluminum with water. Furthermore, only 1 to 2 mils of aluminum is required to stop secondary neutron recoils.

Construction of the 19-plate element presents no manufacturing problems. Several full-sized units were prepared to establish the dimensions, and each unit met specifications in all respects. Also, an enriched fuel element was fabricated for service in the LITR.

The possibility of lowering the aluminum cladding to 10 mils was checked, but analysis revealed that the water-flow area would increase appreciably, that is, by 14.5%.

Results of this and the other modifications discussed are summarized in Table 28. For comparative purposes, cross-sectional views of the present, thin side-plate units and of the 19-plate fuel element are shown in Fig. 20.

The cladding was dropped in increments of 5 mils so that the commercially available, aluminum-stock gages could be used in the Alcladding operation. Actually, the cladding could be reduced in increments of, say, 1 mil but this would require an additional rolling operation and, hence, a greater cost per unit.

Proposed Change in the Lower Stainless Steel Section of the Shim Control Rod. It is proposed to replace the lower stainless steel section in the shim control rod with an aluminum extrusion to reduce fabrication cost. This lower bearing section is presently being fabricated from type 304 stainless steel flat stock that must be machined, welded, stress-relieved, and remachined prior to assembly. Replacing this item with a 63S-grade aluminum extrusion would eliminate most of the costly labor operations.

The effect of this change on operational control, as well as on the mechanical stability of the new rod, was investigated by Gall.[3] Changes in magnet release and drop time were calculated. Also, the stresses produced in the proposed aluminum member by shock on the rod when dropped with full water flow were checked by two methods of analysis.

In conclusion, the study predicted that the change would: (1) decrease the fabrication cost by approximately $300, (2) increase the drop plus magnet release time, under conditions of no water flow, by 10%, (3) produce a stress in the aluminum extrusion, caused by shock on the rod when dropped at full water flow, of less magnitude than exists in the bottom of the fuel section of the existing design. These predicted effects should be confirmed by conducting drop tests. Specifications on the new, aluminum, lower section are given in engineering drawing TD-3038.

MTR Replacement Fuel and Control Rod Elements. The 13 reactor loadings of standard ($\frac{3}{16}$-in.-thick side plates and 60-mils-thick active plates) enriched fuel and control elements on order for calendar year 1952 were completed according to specifications and shipped to Arco.

---

[3] W. R. Gall, *MTR Shim Rod Aluminum Lower Bearing Section*, ORNL CF-52-11-216 (Nov. 29, 1952).

Y-8574

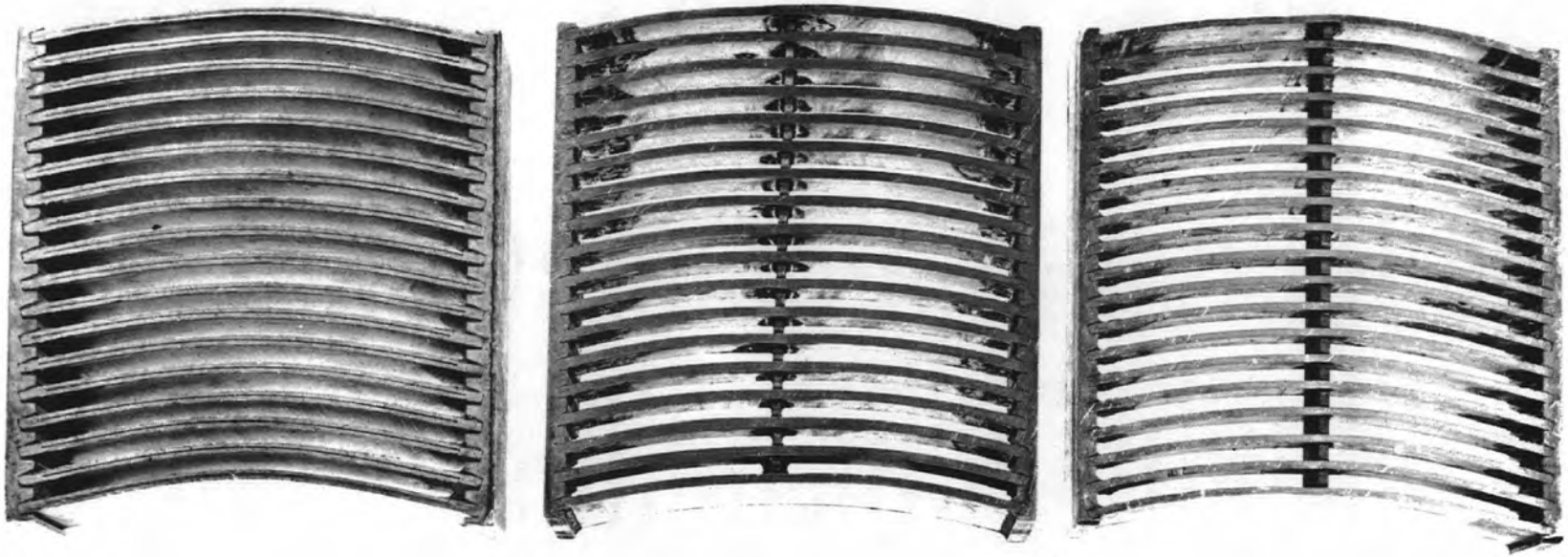

STANDARD 18-PLATE UNIT

Al TO H_2O RATIO = 0.716

THIN SIDE-PLATE UNIT

Al TO H_2O RATIO = 0.667

NEW 19-PLATE UNIT

Al TO H_2O RATIO = 0.565

10 0 1 2

Fig. 20. Cross-Sectional View of Present and Modified MTR Fuel Assemblies.

Shipment on the last loading was made early in December. In addition, three, spare, beryllium-cadmium control rods were fabricated and forwarded.

An experimental loading of "sweetened" fuel elements was completed and shipped to the site in time for the scheduled February 1, 1953 reloading date. These units were fabricated according to specifications determined in discussions at the December meeting, ⅛-in.-thick aluminum side plates with shallow-groove joints were used, and the side plates were flooded with an excess of flux and brazed at a slightly higher temperature than that normally used.

Inspection revealed that all 23 units were well within dimensional tolerance. The maximum deviation of water-gap spacing, for instance, was approximately 117 ± 0.006 mils, or to within ±5% of the specified spacing and the average deviation was about ±3%.

Convair Fuel and Control Rod Elements. The initial loading of enriched uranium-aluminum alloy

TABLE 28. AREAS AND VOLUMES OF MATERIALS IN THE MTR ACTIVE LATTICE FOR SEVERAL FUEL UNIT DESIGNS FOR THE 3- BY 9-SLAB LATTICE 23.622 in. (60 cm) IN LENGTH

Fuel Unit Description						
No. of fuel plates	18	18	18	19	19	20
Side-plate thickness, in.	0.188	0.125	0.125	0.125	0.125	0.125
Cladding-core-cladding thickness, mils	20-20-20	20-20-20	15-20-15	15-20-15	10-20-10	10-20-10
Water-gap spacing, in.	0.117	0.117	0.128	0.118	0.129	0.118
Al-to-H_2O ratio	0.716	0.667	0.529	0.565	0.439	0.464
Areas and Volumes of Materials in Lattice*						
Aluminum						
Area, in.^{2}	111.747	107.929	95.923	99.189	86.861	89.460
Volume, in.^{3}	2639.688	2549.499	2265.893	2343.043	2051.831	2113.224
Water						
Area, in.^{2}	152.797	156.615	168.621	165.332	177.660	175.015
Volume, in.^{3}	3609.371	3699.560	3983.165	3905.473	4196.685	4134.204
Increase in area, %		2.5	10.4	8.2	16.3	14.5
Al-to-H_2O ratio	0.731	0.689	0.569	0.600	0.489	0.511
U^{235}						
Area, in.^{2}	0.607	0.607	0.607	0.628	0.628	0.671
Volume, in.^{3}	14.339	14.339	14.339	14.835	14.835	15.850
U^{234}						
Area, in.^{2}	0.007	0.007	0.007	0.007	0.007	0.008
Volume, in.^{3}	0.165	0.165	0.165	0.165	0.165	0.189
U^{238}						
Area, in.^{2}	0.037	0.037	0.037	0.039	0.039	0.041
Volume, in.^{3}	8.740	8.740	8.740	9.213	9.213	9.685
Total uranium						
Area, in.^{2}	0.651	0.651	0.651	0.674	0.674	0.720
Multiplication Constants						
k_∞	1.682	1.079	1.6711	1.685	1.677	1.702
k_{eff}	1.218	1.227	1.253	1.256	1.277	1.289

*Total area in active core = 9.2137 × 28.7827 = 265.195 in.^{2}

Total volume in active core = 265.195 × 23.622 = 6264.44 in.^{3}

fuel elements for the reactor at Consolidated Vultee Aircraft Corp. has been manufactured and packaged for shipment. The loading consists of 30 of the standard, Bulk Shielding Reactor type of fuel element, 4 special fuel sections to house control rods, and 3 partial units containing 5, 9, and 14 active plates.

Unfortunately, delivery of the units has been delayed for over a month awaiting proper authorization for shipment. The units are being stored in a vault for safe keeping until authorization for shipment is received.

NAA Alclad Uranium-Aluminum Alloy Plates. During the quarter, work was initiated on an order for 330 Alclad uranium-aluminum alloy plates for physical mockup tests at North American Aviation, in connection with the Uranium-Converter Reactor. Some trouble is being experienced in manufacturing these high-uranium-content plates because of segregation during solidification of the alloy.

Nine-pound melts of 26 to 27 wt % uranium were prepared by the direct alloying method and cast into tilted graphite molds. Analysis of samples taken from the casting revealed a 1 to 1.5% variation in uranium content from top to bottom of the castings, as well as some side-to-side segregation. Tolerance on the uranium content in each core is stringent, that is, 8.79 ± 0.08 grams.

Despite the segregation problem, an attempt is being made to obtain alloy cores that are within the tolerance by using the density method. An experimental plot of density of the alloy as a function of composition has been obtained. This curve agrees well with the theoretical curve, except that it is slightly displaced. By determining the density of the individual cores, the uranium content in each core can be obtained from the curve.

Methods of reducing segregation in this alloy are being investigated. Such expedients as chill casting in cast iron, thinner cross section molds, and a 0.2% addition of titanium to the melt have failed to greatly reduce the amount of segregation encountered.

In preliminary tests, the possibility of preparing high-uranium-content plus aluminum compacts by powder metallurgy techniques appears to be promising. Cores of the MTR type, prepared by cold pressing a mixture of U_3O_8 and high-purity aluminum powder, show densities of the order of 90 to 95% of theoretical. Uranium oxide in the form of U_3O_8 is preferred because of its stability to the thermal treatment required during the subsequent jacketing and cladding operations that are done in air.